



# An extracellular acidic cleft confers profound H<sup>+</sup>-sensitivity to epithelial sodium channels containing the $\delta$ -subunit in *Xenopus laevis*

Received for publication, March 2, 2019, and in revised form, June 27, 2019. Published, Papers in Press, June 27, 2019, DOI 10.1074/jbc.RA119.008255

Lukas Wichmann<sup>‡§</sup>, Jasdip Singh Dulai<sup>‡</sup>, Jon Marles-Wright<sup>‡</sup>, Stephan Maxeiner<sup>¶</sup>, Pawel Piotr Szczesniak<sup>||</sup>, Ivan Manzini<sup>§</sup>, and Mike Althaus<sup>‡1</sup>

From the <sup>‡</sup>School of Natural and Environmental Sciences, Newcastle University, Newcastle upon Tyne NE1 7RU, United Kingdom, the <sup>¶</sup>Institute of Anatomy and Cell Biology, Saarland University, 66421 Homburg, Germany, the <sup>||</sup>Department of Medicine, Haematology/Oncology, Johann-Wolfgang-Goethe University Frankfurt, 60323 Frankfurt, Germany, and the <sup>§</sup>Institute of Animal Physiology, Department of Animal Physiology and Molecular Biomedicine, Justus-Liebig University Giessen, 35390 Giessen, Germany

Edited by Mike Shipston

The limited sodium availability of freshwater and terrestrial environments was a major physiological challenge during vertebrate evolution. The epithelial sodium channel (ENaC) is present in the apical membrane of sodium-absorbing vertebrate epithelia and evolved as part of a machinery for efficient sodium conservation. ENaC belongs to the degenerin/ENaC protein family and is the only member that opens without an external stimulus. We hypothesized that ENaC evolved from a proton-activated sodium channel present in ionocytes of freshwater vertebrates and therefore investigated whether such ancestral traits are present in ENaC isoforms of the aquatic pipid frog *Xenopus laevis*. Using whole-cell and single-channel electrophysiology of *Xenopus* oocytes expressing ENaC isoforms assembled from  $\alpha\beta\gamma$ - or  $\delta\beta\gamma$ -subunit combinations, we demonstrate that *Xenopus*  $\delta\beta\gamma$ -ENaC is profoundly activated by extracellular acidification within biologically relevant ranges (pH 8.0–6.0). This effect was not observed in *Xenopus*  $\alpha\beta\gamma$ -ENaC or human ENaC orthologs. We show that protons interfere with allosteric ENaC inhibition by extracellular sodium ions, thereby increasing the probability of channel opening. Using homology modeling of ENaC structure and site-directed mutagenesis, we identified a cleft region within the extracellular loop of the  $\delta$ -subunit that contains several acidic amino acid residues that confer proton-sensitivity and enable allosteric inhibition by extracellular sodium ions. We propose that *Xenopus*  $\delta\beta\gamma$ -ENaC can serve as a model for investigating ENaC transformation from a proton-activated toward a constitutively-active ion channel. Such transformation might have occurred during the evolution of tetrapod vertebrates to enable bulk sodium absorption during the water-to-land transition.

Water-to-land transition was a key event in the evolution of tetrapod vertebrates. By transitioning into terrestrial habitats,

The authors declare that they have no conflicts of interest with the contents of this article.

This article contains Table S1.

<sup>1</sup>To whom correspondence should be addressed: School of Natural and Environmental Sciences, Newcastle University, Ridley Bldg. 2, Newcastle upon Tyne NE1 7RU, United Kingdom. Tel.: 44-191-208-4700; E-mail: mike.althaus@newcastle.ac.uk.

tetrapod ancestors faced major physiological challenges, such as the need for breathing air, as well as a limited availability of water and sodium. Mechanisms that permitted sodium absorption from a sodium-scarce environment are likely to have evolved while vertebrate ancestors invaded freshwater habitats. This suggests that tetrapod ancestors were likely equipped with a molecular machinery allowing them to evolve efficient mechanisms for bulk sodium and, consequently, water conservation.

Although comparative physiological studies reveal evolutionary adaptations at an organ level (1), not much is known about functional adaptations of proteins required for sodium and water conservation. In tetrapod vertebrates, a key protein for conserving sodium is the epithelial sodium channel (ENaC).<sup>2</sup> The presence of ENaC genes in modern jawless vertebrates (2) suggests that ENaC evolved early within the vertebrate lineage. In sodium-absorbing epithelia of tetrapod vertebrates, ENaC is located in the apical epithelial membrane and is rate-limiting for the uptake of sodium ions into epithelial cells. In conjunction with basolateral Na<sup>+</sup>/K<sup>+</sup>-ATPases, ENaC facilitates the vectorial absorption of sodium ions, which also generates osmotic forces that drive water absorption (3). In humans, an increased volume of airway surface liquid as well as urinary salt-loss in patients suffering from type 1 pseudohypoadosteronism are clinical manifestations of ENaC loss-of-function mutations mirroring insufficient adaptation to terrestrial life (4). In severe cases, patients require a daily uptake of 18 g of sodium (2) as compared with a recommended daily value of a maximum of 1.5 g (5).

Canonical ENaCs assemble as heterotrimers consisting of three homologous subunits ( $\alpha$ ,  $\beta$ , and  $\gamma$ ). A fourth  $\delta$ -subunit can replace the  $\alpha$ -subunit and form heteromeric ENaCs with different biophysical and functional properties (6). A recent study resolving the structure of human  $\alpha\beta\gamma$ -ENaC revealed that each subunit contains short intracellular N and C termini that are connected by two transmembrane helices and a large extracellular domain (7). The topology of this ectodomain resembles a clenched hand comprising the “palm,” “knuckle,”

<sup>2</sup>The abbreviations used are: ENaC, epithelial sodium channel; ANOVA, analysis of variance; ASIC, acid-sensing ion channel; SSI, sodium self-inhibition; PDB, Protein Data Bank; TEVC, two-electrode voltage-clamp; NMDG, N-methyl-D-glucamine.

## pH-sensitivity of *Xenopus* $\delta$ -ENaC

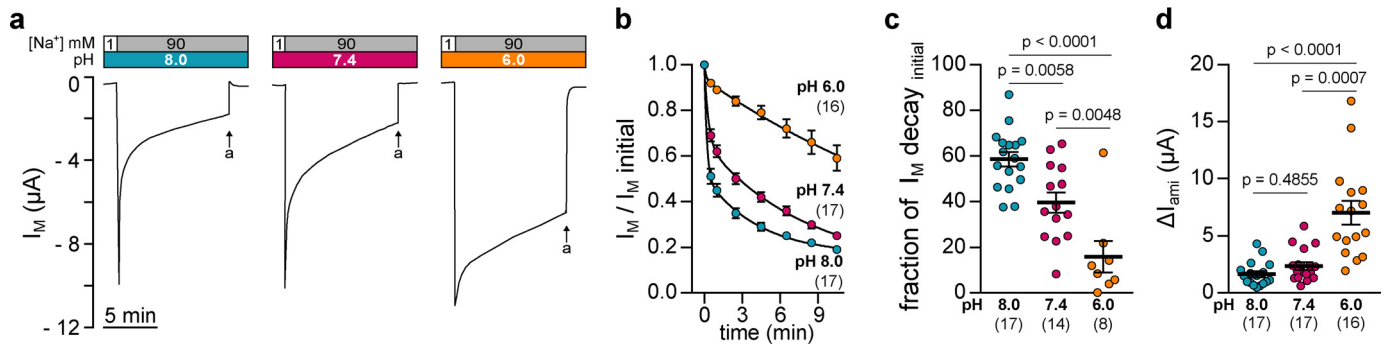


**Figure 1. Extracellular pH modifies *Xenopus*  $\delta\beta\gamma$ -ENaC currents.** *a*, representative recordings of transmembrane currents ( $I_M$ ) in oocytes expressing *Xenopus*  $\delta\beta\gamma$ -ENaC. The extracellular pH alters transient current kinetics of *Xenopus*  $\delta\beta\gamma$ -ENaC. Arrows indicate application of amiloride (a, 100  $\mu$ M). *b*, current decays normalized to the initial peak values ( $I_{M, \text{initial}}$ ) from recordings as depicted in *a* follow a two-phase decay consisting of a fast, initial decay as well as a slow, continuous current rundown. *c*, fractions of the fast, initial current decay ( $I_{M, \text{decay, initial}}$ ) are reduced with decreasing extracellular pH (one-way ANOVA,  $F = 20.31$ ,  $p < 0.0001$ ; Tukey's multiple comparisons test). *d*, amiloride-sensitive current fractions ( $\Delta I_{\text{ami}}$ ) derived from recordings as shown in *a* are markedly increased at pH 6.0 (Kruskal-Wallis test,  $p < 0.0001$ ; Dunn's multiple comparisons test).

“finger,” and “thumb” domains, surrounding a central “ $\beta$ -ball.” Aside from the ENaC-specific GRIP (gating relief of inhibition by proteolysis) domain, which confers channel sensitivity to proteolytic activation, this structural organization is similar to that of acid-sensing ion channels (ASICs) (7). However, despite a shared channel architecture, representatives of the degenerin/ENaC family are functionally distinct, as they open in response to various external stimuli (8). This includes mechanosensitive degenerin channel complexes in *Caenorhabditis elegans* (9), peptide-gated channels in molluscs (10), and proton-sensitive ASICs (11). ENaC emerged in vertebrates and is the only member of this protein family that opens without an external stimulus, representing an evolutionary adaptation for bulk sodium absorption. The molecular changes that enabled an evolutionary transition from a stimulus-activated ancestor to a constitutively-active ENaC are unknown. Many freshwater vertebrates absorb sodium ions from the environment by specialized gill epithelial cells (ionocytes) that secrete protons via apical vacuolar-type  $H^+$ -ATPases (12). Protons are either used to co-transport sodium ions into ionocytes via proton-coupled sodium transporters or sodium-permeable ion channels that open in response to apical extracellular acidification (12).

We hypothesize that ENaC evolved from an ancestral ion channel that was originally opened in response to protons and then progressed to constitutive activity during water-to-land transition. At a molecular level, this hypothesis is supported by the close evolutionary relationship and the structural similarities between ENaC and proton-gated ASICs, which are evolutionarily older. ASICs recently have been suggested as possible candidates for proton-coupled sodium uptake in ionocytes of freshwater zebrafish (12) and rainbow trout (13). Furthermore, mammalian ENaCs are sensitive to extracellular pH in a species-specific manner, as exemplified by a 40% increase in human  $\alpha\beta\gamma$ -ENaC activity due to extracellular acidification (pH 6.0) (14). Precedents for evolutionary gain or loss of proton-sensitivity within vertebrate degenerin/ENaC proteins have recently been demonstrated for ASIC1, which gained proton-sensitivity during the emergence of bony fishes (15), and ASIC4, which lost proton-sensitivity in the mammalian lineage (16).

We and others (17) have recently shown that  $\delta\beta\gamma$ -ENaC in the South African clawed frog *Xenopus laevis* generates sodium currents, which have a more transient form compared with those generated by  $\alpha\beta\gamma$ -ENaC. This is the only ENaC ortholog characterized to date that displays such characteristics. The transient nature is due to a slow but profound inhibition of ENaC activity by extracellular sodium ions, a mechanism called sodium self-inhibition (SSI) (17, 18). Various cues such as acidic pH (14) or proteases (19) have been shown to increase ENaC activity by uncoupling channels from SSI. Because *Xenopus* ENaCs containing the  $\delta$ -ENaC subunit are insensitive to proteolytic activation (18), we hypothesized that the enhanced SSI of *Xenopus*  $\delta\beta\gamma$ -ENaC enables channel activation through extracellular acidification. This ENaC isoform might therefore exhibit functional characteristics of a proton-stimulated ENaC ancestor.

We demonstrate that, in contrast to canonical *Xenopus*  $\alpha\beta\gamma$ -ENaC,  $\delta$ -ENaC-containing channels are profoundly activated by extracellular acidification. Modulation of  $\delta\beta\gamma$ -ENaC activity within physiological pH ranges (pH 8.0–6.0) involves changes in single-channel open probability and SSI. Substitutions of single aspartates in an acidic cleft located at the interface between the  $\delta$ -ENaC knuckle and finger domains significantly alter  $\delta\beta\gamma$ -ENaC sensitivity to pH and SSI, suggesting convergence of channel regulation by extracellular protons and sodium within this region. These findings suggest that *Xenopus*  $\delta\beta\gamma$ -ENaC might be a functional model that represents the junction between constitutively active ENaCs and cognate proton-gated ion channels within the degenerin/ENaC family. Consequently, this amphibian ENaC isoform may provide insight into the evolutionary transition between gating modes that may have occurred during water-to-land transition of tetrapod vertebrates.

## Results

### Activity of *Xenopus* $\delta\beta\gamma$ -ENaC is sensitive to changes in the extracellular pH

The effect of extracellular acidification on *Xenopus*  $\delta\beta\gamma$ -ENaC activity was functionally characterized by microelectrode recordings, employing the *Xenopus* oocyte expression

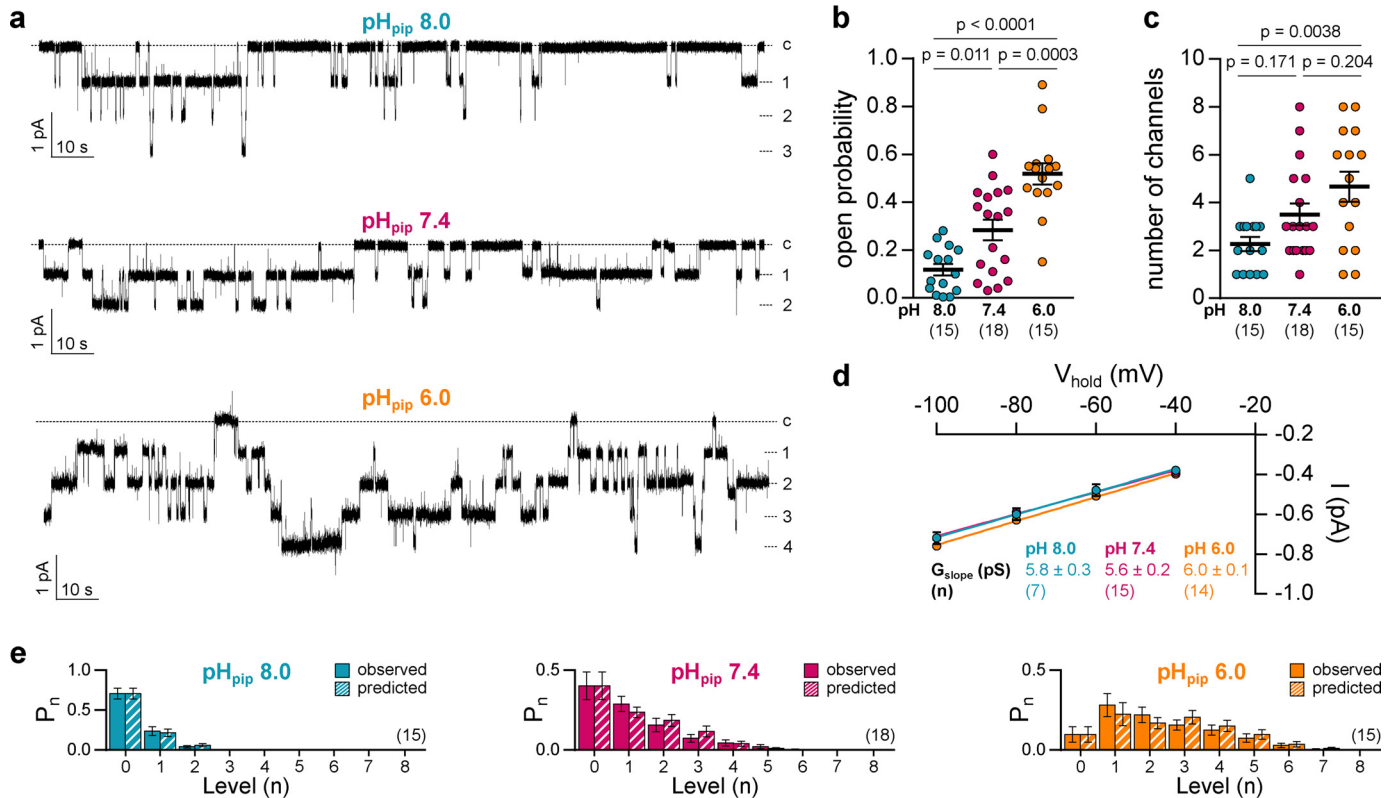


**Figure 2. Extracellular pH affects gating of *Xenopus*- $\delta\beta\gamma$ -ENaC.** *a*, representative current traces from cell-attached patch-clamp recordings of oocytes expressing *Xenopus*  $\delta\beta\gamma$ -ENaC at a holding potential of  $-100$  mV. Recordings were performed using pipette solutions at pH 8.0, 7.4, or 6.0 ( $\text{pH}_{\text{pip}}$ ). Dashed lines indicate the number of individual open channel levels or the current baseline (c). *b*, open probability of individual channels increases with decreasing  $\text{pH}_{\text{pip}}$  (one-way ANOVA,  $F = 24.93$ ,  $p < 0.0001$ ; Tukey's multiple comparisons test). *c*, number of visible channels in cell-attached recordings as depicted in *a* (one-way ANOVA,  $F = 5.83$ ,  $p = 0.0056$ ; Tukey's multiple comparisons test). *d*, current ( $I$ )/voltage ( $V_{\text{hold}}$ ) plots derived from cell-attached patch-clamp recordings of *Xenopus*  $\delta\beta\gamma$ -ENaC at different  $\text{pH}_{\text{pip}}$ . The  $\text{pH}_{\text{pip}}$  does not affect the channel's slope conductance ( $G_{\text{slope}}$ ) (one-way ANOVA,  $F = 1.854$ ,  $p = 0.1725$ ), which was calculated from the linear regression of unitary channel conductance (mean of at least three single channel amplitudes per  $n$ ) at  $-40$  to  $-100$  mV. *e*, estimation of the number of channels in the patch.  $P_n$  is the probability of  $n$  channels out of the total number of channels within the patch being opened. The observed probability for each  $n$  (i.e. observed current levels) was compared with a theoretical distribution of  $P_n$ , as predicted by a binomial distribution, assuming  $n$  channels present in the patch. There is no significant difference between observed and predicted  $P_n$  values under the employed  $\text{pH}_{\text{pip}}$  conditions (Kruskal-Wallis test with Dunn's multiple comparisons test in each panel.  $p > 0.9999$  between each pair of  $P_n$  observed and  $P_n$  predicted.). Statistical evaluation is based on individual recordings lasting for 120–180 s with a maximum of eight channels per patch. Please note that single-channel characteristics at  $\text{pH}_{\text{pip}}$  7.4 include data, which have been reported earlier (18). Patch-clamp data for both studies were collected simultaneously using the same oocyte batches for all pH conditions and  $\alpha\beta\gamma$ - as well as  $\delta\beta\gamma$ -ENaC.

system at a holding potential ( $V_M$ ) of  $-60$  mV. We and others have previously demonstrated a transient nature of transmembrane currents ( $I_M$ ) mediated by *Xenopus* ENaC containing the  $\delta$ -subunit after washout of the ENaC blocker amiloride or a rapid increase in the extracellular sodium concentration (17, 18). As illustrated in Fig. 1, this characteristic decay of  $I_M$  in oocytes expressing *Xenopus*  $\delta\beta\gamma$ -ENaC was altered depending on the extracellular pH. Changing the extracellular sodium concentration ( $[\text{Na}^+]$ ) from 1 to 90 mM at pH 7.4, elicited a rapid increase of  $I_M$  that was followed by an initial, fast decline and a subsequent slow but continuous rundown (Fig. 1a). Current levels normalized to the initial peak in  $I_M$  followed a two-phase decay function (Fig. 1b), where  $39.6 \pm 3.1\%$  ( $n = 14$ ) of the total current decline was attributable to the initial fraction of  $I_M$  decay (Fig. 1c). Although this two-phase current decline was also observed at an alkaline pH of 8.0, the fraction of the initial  $I_M$  decay under these conditions was significantly enhanced ( $58.5 \pm 3.1\%$ ;  $p = 0.0058$ ;  $n = 17$ ). In contrast, acidification of the extracellular solution to pH 6.0 markedly reduced the fraction of this initial  $I_M$  decay ( $15.9 \pm 6.9\%$ ;  $p = 0.0048$ ;  $n = 8$ ) culminating in increased amiloride-sensitive

current fractions ( $\Delta I_{\text{ami}}$ ) mediated by *Xenopus*  $\delta\beta\gamma$ -ENaC under acidic conditions (Fig. 1d). Changes in the extracellular pH did not affect the magnitude of the initial peak in  $I_M$  ( $I_{M, \text{peak}}$ :  $-11.0 \pm 1.6 \mu\text{A}$  at pH 8.0,  $-10.3 \pm 1.1 \mu\text{A}$  at pH 7.4, and  $-12.5 \pm 1.1 \mu\text{A}$  at pH 6.0; one-way ANOVA,  $F = 0.7822$ ,  $p = 0.4632$ ). These results indicate that the extracellular pH influences the activity of *Xenopus*  $\delta\beta\gamma$ -ENaC and alters current kinetics at the whole-cell level.

We next examined the effect of extracellular acidification on  $\delta\beta\gamma$ -ENaC at the single channel level. Cell-attached patch-clamp recordings lasting for 120–180 s at  $V_{\text{hold}} = -100$  mV were performed using pipette solutions with pH values ( $\text{pH}_{\text{pip}}$ ) of 8.0, 7.4, and 6.0 (Fig. 2). Individual channels displayed a low open probability ( $P_o$ ) at  $\text{pH}_{\text{pip}}$  8.0 ( $0.12 \pm 0.02$ ,  $n = 15$ ), whereas  $P_o$  increased to a moderate level at  $\text{pH}_{\text{pip}}$  7.4 ( $0.24 \pm 0.04$ ;  $p = 0.011$ ;  $n = 18$ ) and was further enhanced at  $\text{pH}_{\text{pip}}$  6.0 ( $0.52 \pm 0.04$ ;  $p = 0.0003$ ;  $n = 15$ ; Fig. 2b). The number of visible channels was increased in recordings performed at  $\text{pH}_{\text{pip}}$  6.0 when compared with alkaline conditions at  $\text{pH}_{\text{pip}}$  8.0 (Fig. 2c); however, a low  $P_o$  at  $\text{pH}_{\text{pip}}$  8.0 might lead to underestimation of channel abundance. The slope conductance ( $G_{\text{slope}}$ ) of  $\delta\beta\gamma$ -



## pH-sensitivity of *Xenopus* $\delta$ -ENaC

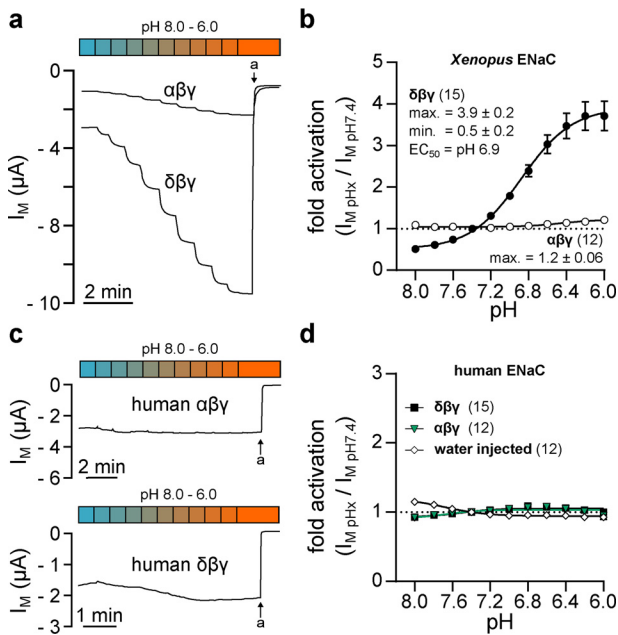


**Figure 3. *Xenopus*  $\delta\beta\gamma$ -ENaC is activated by extracellular acidification.** *a*, recordings of  $I_M$  in oocytes expressing *Xenopus*  $\alpha\beta\gamma$ - or  $\delta\beta\gamma$ -ENaC. Amiloride-sensitive (*a*, amiloride, 100  $\mu\text{M}$ ) currents mediated by  $\delta\beta\gamma$ - but not  $\alpha\beta\gamma$ -ENaC are dose-dependently increased by a stepwise acidification of the extracellular solution (pH 8.0–6.0; pH 0.2 increments). *b*, dose-response curves of acid-mediated activation of *Xenopus* ENaC isoforms. Normalized ( $I_{M, \text{pH}x} / I_{M, \text{pH}7.4}$ ) current levels were fit to a sigmoidal dose-response function with variable slope (Hill-slope of *Xenopus*  $\delta\beta\gamma$ -ENaC:  $1.6 \pm 0.4$ ). Compared with pH 7.4, alkaline conditions decrease channel activity to a minimal factor (*min.*) of  $0.5 \pm 0.2$ , whereas acidification enhances activity of  $\delta\beta\gamma$ -ENaC by a maximal factor (*max.*) of  $3.9 \pm 0.2$ . *c* and *d*, maximal acid-induced activation of currents mediated by human  $\alpha\beta\gamma$ -ENaC (*max.*:  $1.03 \pm 0.01$ ) or  $\delta\beta\gamma$ -ENaC (*max.*:  $1.05 \pm 0.01$ ) is considerably reduced with respect to *Xenopus*  $\delta\beta\gamma$ -ENaC.

ENaC was derived from linear regression of unitary channel conductance at  $V_{\text{hold}}$  from  $-40$  to  $-100$  mV. The  $\text{pH}_{\text{pip}}$  did not significantly affect the  $G_{\text{slope}}$  of the channel (Fig. 2*d*; one-way ANOVA,  $F = 1.854$ ,  $p = 0.1725$ ). Taken together, these results indicate that pH-mediated modulation of *Xenopus*  $\delta\beta\gamma$ -ENaC activity is based on changes in channel  $P_o$ .

### The $\delta$ -subunit confers a pronounced pH-sensitivity to *Xenopus* ENaC

The magnitude of stimulation of *Xenopus*  $\delta\beta\gamma$ -ENaC by extracellular acidification was compared with channels containing the  $\alpha$ -ENaC subunit ( $\alpha\beta\gamma$ ) from *X. laevis* as well as both human channel orthologs ( $\delta\beta\gamma$ - and  $\alpha\beta\gamma$ -ENaC). As depicted in Fig. 3*a*, stepwise acidification of the extracellular solution from pH 8.0 to 6.0 in increments of pH 0.2 resulted in a successive increase of  $I_M$  in oocytes expressing *Xenopus*  $\delta\beta\gamma$ -ENaC that reached a maximum between pH 6.4 and 6.0 and was sensitive to amiloride. The dose-response relationship of individual current levels normalized to  $I_M$  at pH 7.4 indicated a maximal activation of the channel by a factor of  $3.9 \pm 0.2$  under acidic conditions, whereas alkaline pH reduced ENaC activity to a factor of  $0.5 \pm 0.2$  ( $n = 15$ ). The sigmoidal dose-response curve exhibited a Hill-slope of  $1.6 \pm 0.4$  and a half-maximal channel activation ( $\text{EC}_{50}$ ) at pH 6.9 (Fig. 3*b*). Alkaline inhibition, maximal acidic activation, as well as the  $\text{EC}_{50}$  and Hill-slope of *Xenopus*  $\delta\beta\gamma$ -ENaC were not significantly different

when  $\text{H}_2\text{SO}_4$  was employed for pH titration instead of HCl (data not shown). In *Xenopus* ENaC containing the  $\alpha$ -subunit, maximal acid-induced channel activation was significantly reduced to a factor of  $1.2 \pm 0.06$  ( $n = 12$ ), while there was no channel inhibition at alkaline pH. Moreover, pH-mediated channel regulation between pH 8.0 and 6.0 was also reduced in human ENaC isoforms (Fig. 3, *c* and *d*). Human  $\delta\beta\gamma$ -ENaC displayed a maximal acid-induced fold-activation of  $1.05 \pm 0.01$  and an alkaline inhibition to a factor of  $0.93 \pm 0.04$  ( $n = 12$ ), whereas in  $\alpha\beta\gamma$ -ENaC these values were  $1.03 \pm 0.01$  and  $0.9 \pm 0.1$  ( $n = 11$ ), respectively. These results demonstrate that the presence of the  $\delta$ -subunit facilitates a markedly pronounced pH-sensitivity in *Xenopus* ENaC that is not found in either isoform of orthologous human channels. As  $I_M$  recorded in water-injected oocytes was not reduced at alkaline pH or enhanced under acidic conditions, the involvement of endogenous channels or transporters in the observed pH-mediated changes of  $I_M$  can be excluded.

### Changes in the extracellular pH modulate ENaC sodium self-inhibition

Transmembrane currents mediated by ENaC are generally subject to a time-dependent decay that is attributable to two distinct mechanisms. SSI describes an immediate, allosteric reduction of ENaC  $P_o$  in the presence of high extracellular sodium concentrations (20). The more slowly-progressing feedback inhibition involves a reduction of channel  $P_o$  and internalization of membrane resident ENaCs due to accumulation of intracellular  $\text{Na}^+$  (21). Because previous reports have suggested that ENaC activation by acidic pH is predominantly associated with a reduced SSI (14), we hypothesized a similar correlation in *Xenopus*  $\delta\beta\gamma$ -ENaC, which is characterized by a markedly pronounced SSI (17, 18). Fig. 4 illustrates a similar reversibility and magnitude of acid-induced activation and SSI of  $\delta\beta\gamma$ -ENaC as well as an apparent independence of both mechanisms from the slowly progressing decline of  $I_M$  over time. Increasing extracellular  $[\text{Na}^+]$  from 1 to 90 mM at pH 7.4 induced a peaked increase in  $I_M$  that was followed by a rapid, initial current decay and a subsequent slow current rundown (Fig. 4*a*, also see Fig. 1). During this current rundown, extracellular acidification (pH 6.0 for 30 s) reversibly activated a consistent fraction of  $I_M$  that did not decrease but slightly increased over time (Fig. 4*b*). The observed increase of pH 6.0 sensitive  $I_M$  fractions can be mainly attributed to a reduced magnitude of the first acid-induced current increase, which may originate from an overlap with the strong, initial current decay. Notably, the magnitudes of SSI (measured as current fractions lost after 3 min of SSI) were constant over time when SSI was repetitively induced (Fig. 4, *c* and *d*) supporting a functional correlation between ENaC activation by acidic pH and inhibition through SSI. To examine a functional interdependence between  $\text{Na}^+$ -mediated inhibition and acid-induced activation of ENaC, we assessed the  $\text{Na}^+$  dependence of channel activation due to extracellular acidification. As presented in Fig. 4, *e* and *f*, the half-maximal proton-induced activation (pH  $\text{EC}_{50}$ ) of *Xenopus*  $\delta\beta\gamma$ -ENaC depended on the extracellular  $\text{Na}^+$  concentration. Reduction of the extracellular  $[\text{Na}^+]$  dose-dependently shifted the channel's pH  $\text{EC}_{50}$  to more alkaline values, suggesting that

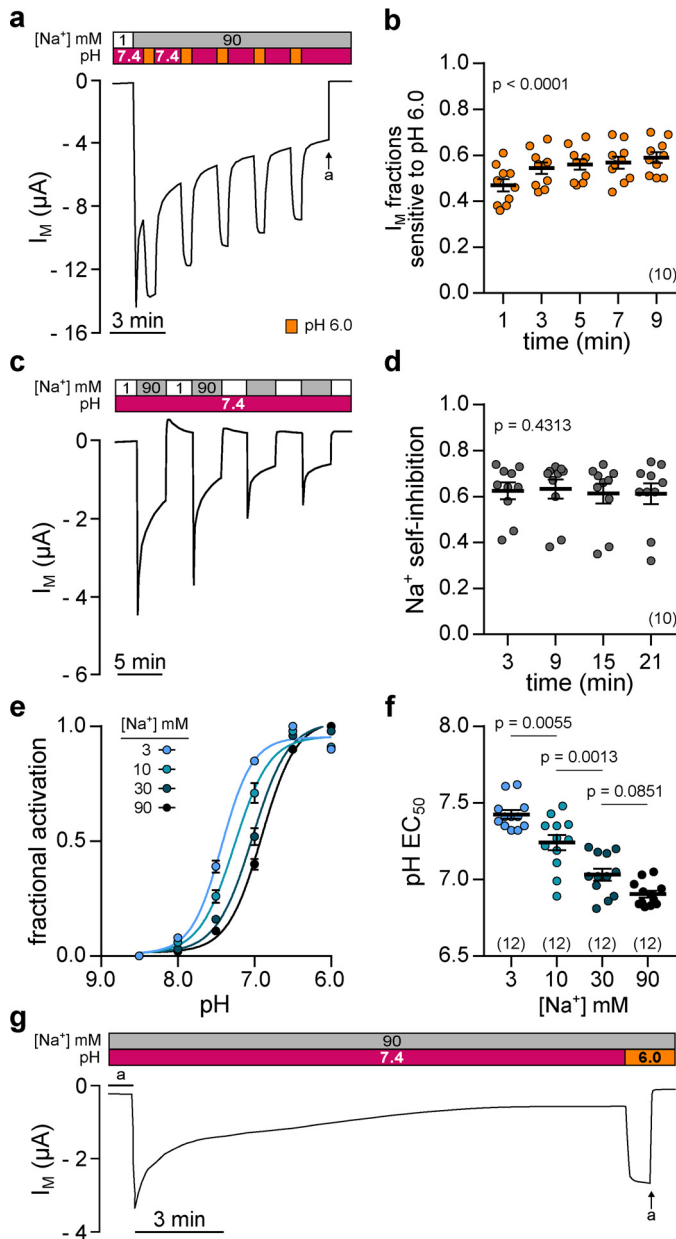


**Figure 4. Acidic pH elicits a reversible, consistent, and Na<sup>+</sup>-dependent activation of *Xenopus*  $\delta\beta\gamma$ -ENaC.** *a*, representative current trace of an oocyte expressing *Xenopus*  $\delta\beta\gamma$ -ENaC. Repetitive acidification of the extracellular milieu (from pH 7.4 to pH 6.0 for 30 s) reversibly increases  $I_M$  (*a* = amiloride, 100  $\mu$ M). *b*, normalized  $I_M$  fractions sensitive to pH 6.0 ( $(I_{M, \text{pH } 6.0} - I_{M, \text{pH } 7.4})/I_{M, \text{pH } 6.0}$ ) from recordings as depicted in *a*. Acid-sensitive current fractions do not decline but rather increase over time (repeated-measures one-way ANOVA,  $F = 57.8$ ,  $p < 0.0001$ ; Tukey's multiple comparisons test). *c*, assessment of repetitive SSI in an oocyte expressing *Xenopus*  $\delta\beta\gamma$ -ENaC. SSI was defined as the decline in  $I_M$  at 3 min after increasing extracellular  $[\text{Na}^+]$  from 1 to 90 mM. *d*, Na<sup>+</sup> self-inhibition values from recordings as depicted in *c*. Current fractions lost to SSI ( $(I_{M, \text{peak}} - I_{M, 3 \text{ min}})/I_{M, \text{peak}}$ ) are constant over time (repeated-measures one-way ANOVA,  $F = 0.8537$ ,  $p = 0.4313$ ; Tukey's multiple comparisons test). *e*, Na<sup>+</sup> dependence of acid-induced ENaC activation was examined through determination of the pH EC<sub>50</sub> (pH 8.5–6.0; pH 0.5 increments) under different Na<sup>+</sup> concentrations (3–90 mM). Fractional channel activation was calculated as the difference between  $I_M$  at a given pH ( $I_{M, x}$ ) and the minimal  $I_M$  ( $I_{M, \text{min}}$ ) in relation to the maximally observed difference in  $I_M$  ( $\Delta_{\text{max}} I_M$ ) in the respective recording ( $(I_{M, x} - I_{M, \text{min}})/\Delta_{\text{max}} I_M$ ). *f*, alkaline-shift of the pH EC<sub>50</sub> in the presence of reduced  $[\text{Na}^+]$  indicates that less protons are needed for acid-induced channel activation under low  $[\text{Na}^+]$  (one-way ANOVA,  $F = 38.51$ ,  $p < 0.0001$ ; Tukey's multiple comparisons test). *g*, extracellular acidification (from pH 7.4 to pH 6.0) still activates *Xenopus*  $\delta\beta\gamma$ -ENaC after maximal rundown of currents.

lower concentrations of protons are necessary to maximally activate ENaC at reduced extracellular  $[\text{Na}^+]$ . These results indicate that pH-mediated activation of *Xenopus*  $\delta\beta\gamma$ -ENaC is affected by the extracellular  $\text{Na}^+$  concentration, thus suggesting that protons alter channel activity by modulating SSI. Because SSI of ENaC is only visible during experimental conditions as employed in this study, we additionally examined whether proton-sensitivity is maintained in prolonged recordings, when currents have reached a quasi-steady-state level. Indeed, extracellular acidification (pH 6.0) led to a strong increase of  $I_M$  (Fig. 4g), indicating that pH-sensitivity might also represent a physiologically relevant stimulus activating *Xenopus*  $\delta\beta\gamma$ -ENaC.

To further examine how protons and SSI interact, we determined the effect of extracellular pH on the magnitude and apparent Na<sup>+</sup> affinity of SSI in *Xenopus*  $\delta\beta\gamma$ -ENaC (Fig. 5). SSI was assessed by successively increasing extracellular  $[\text{Na}^+]$  from 1 mM to either 3, 10, 30, 60, 90, or 120 mM for 3 min. Fractional inhibition of  $I_M$  from the initial peak current ( $I_{M, \text{peak}}$ ) to current levels after 3 min ( $I_{M, 3 \text{ min}}$ ) was defined as SSI ( $(I_{M, \text{peak}}/I_{M, 3 \text{ min}})/I_{M, \text{peak}}$ ). Plotting the magnitude of SSI against the respective  $[\text{Na}^+]$  allowed for estimation of maximal inhibition ( $V_{\text{max}}$ ) and apparent Na<sup>+</sup> affinity ( $K_m$ ) of SSI as values followed a Michaelis-Menten relation. Under alkaline conditions (pH 8.0), *Xenopus*  $\delta\beta\gamma$ -ENaC exhibited a maximal SSI of  $0.57 \pm 0.03$ , which was half-maximally reached at  $2.1 \pm 0.4$  mM Na<sup>+</sup> ( $n = 10$ ; Fig. 5a). Although the magnitude of maximal SSI reached a similar value in the presence of pH 7.4 ( $0.55 \pm 0.03$ ,  $p = 0.9502$ ), the Na<sup>+</sup> affinity of SSI was significantly reduced under these conditions ( $K_m = 8.1 \pm 2.2$  mM Na<sup>+</sup>,  $p = 0.0347$ ,  $n = 16$ ; Fig. 5b). Compared with pH 7.4, further extracellular acidification (pH 7.0, Fig. 5c) led to a reduction of maximal SSI ( $0.4 \pm 0.05$ ,  $p = 0.017$ ), whereas the apparent Na<sup>+</sup> affinity ( $K_m = 16.8 \pm 6.8$  mM Na<sup>+</sup>,  $p = 0.9999$ ,  $n = 13$ ) was not significantly changed. In line with results presented in Fig. 1, SSI of *Xenopus*  $\delta\beta\gamma$ -ENaC was altered at pH 6.0 (Fig. 5d). Although the magnitude of channel inhibition was moderate in the presence of 3 mM Na<sup>+</sup> ( $0.29 \pm 0.04$ ), it did not increase with rising sodium concentrations (SSI at 120 mM Na<sup>+</sup> =  $0.14 \pm 0.02$ ,  $n = 10$ ). Because these data did not converge with a Michaelis-Menten fit, estimation of maximal SSI and apparent Na<sup>+</sup> affinity was not feasible. Nevertheless, these data clearly demonstrate that changes in the extracellular pH affect the magnitude and Na<sup>+</sup> affinity of SSI in *Xenopus*  $\delta\beta\gamma$ -ENaC, thus indicating that extracellular protons activate ENaC by antagonizing Na<sup>+</sup>-mediated channel inhibition. This is additionally supported by the synergy/antagonism estimation using an interaction matrix composed of Na<sup>+</sup>- and proton-dependent SSI values of *Xenopus*  $\delta\beta\gamma$ -ENaC (Fig. 5e). The landscape visualizes deviations of the observed values for SSI from a reference model (Bliss model (22)) that assumes a functional independence between the two factors. Negative Bliss values with an average of  $-23.4$  indicate an antagonistic combinational effect, which protons exert on the Na<sup>+</sup>-dependent magnitude of SSI in *Xenopus*  $\delta\beta\gamma$ -ENaC.

## pH-sensitivity of *Xenopus* $\delta$ -ENaC

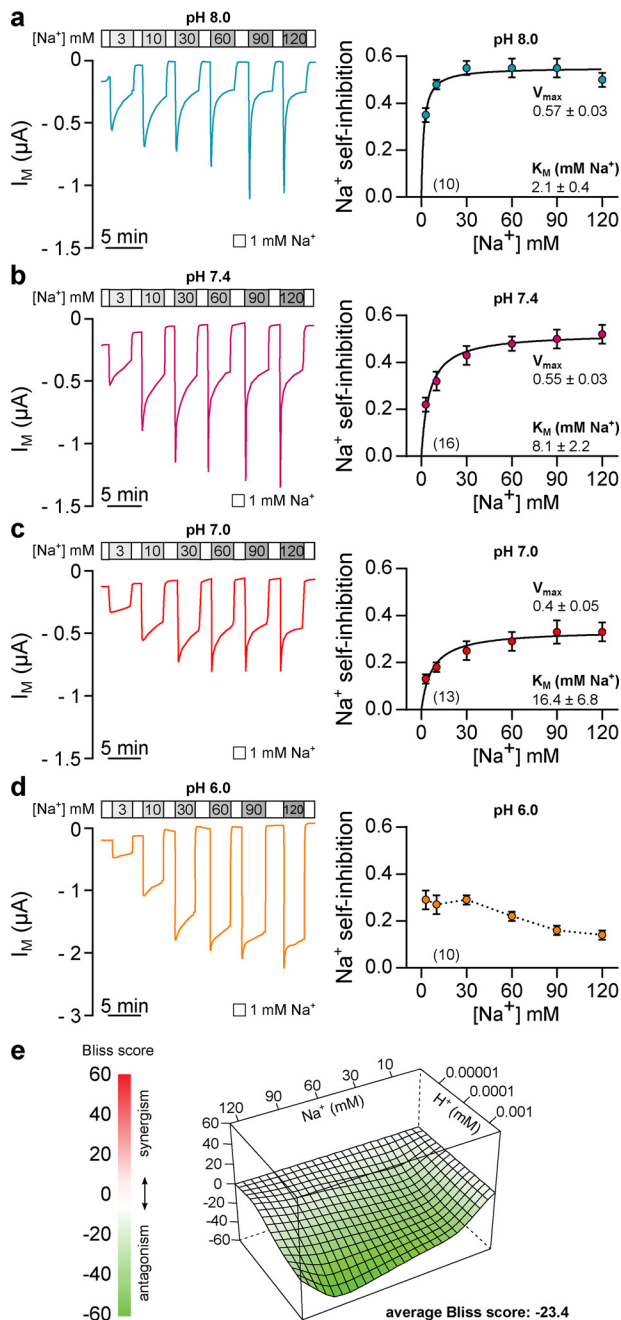


**Figure 5. Extracellular acidification antagonizes sodium self-inhibition of *Xenopus*  $\delta\beta\gamma$ -ENaC.** *a*, representative recording of  $I_M$  in oocytes expressing *Xenopus*  $\delta\beta\gamma$ -ENaC. SSI was determined by rapidly changing extracellular  $[Na^+]$  from 1 to 3–120 mM at pH 8.0. The magnitude of  $Na^+$  self-inhibition ( $(I_{M,peak} - I_{M,3min})/I_{M,peak}$ ) was plotted against the respective  $[Na^+]$  and fitted to the Michaelis-Menten equation, allowing estimation of maximal inhibition ( $V_{max}$ ) and apparent affinity for  $Na^+$  ( $K_M$ ). *b–d*, current recordings and Michaelis-Menten plots of SSI in *Xenopus*  $\delta\beta\gamma$ -ENaC at pH 7.4, 7.0, and 6.0. At pH 8.0,  $V_{max}$  of SSI is similar to values at pH 7.4 (*b*), but SSI displays an enhanced  $Na^+$  affinity (Kruskal-Wallis test,  $p = 0.035$ ; Dunn's multiple comparisons test). Compared with values at pH 7.4, further acidification (pH 7.0, *c*) decreases  $V_{max}$  (one-way ANOVA,  $F = 5.508$ , Tukey's multiple comparisons test,  $p = 0.017$ ), whereas the apparent  $Na^+$  affinity of SSI is not significantly changed (Kruskal-Wallis test, Dunn's multiple comparisons test,  $p > 0.999$ ). Irrespective of the extracellular  $[Na^+]$ , SSI of *Xenopus*  $\delta\beta\gamma$ -ENaC is markedly reduced at pH 6.0 (*d*) and does not converge to a Michaelis-Menten fit. *e*, interaction landscape for  $Na^+$ -dependent SSI at different extracellular  $H^+$ . The Bliss score indicates deviations of the measured combinational responses from a reference model that assumes independence between  $Na^+$ - and  $H^+$ -mediated responses. Negative Bliss values across the interaction landscape indicate antagonism of  $Na^+$  dependent SSI by increasing  $H^+$ .

## Mutations in the "acidic cleft" of the $\delta$ -ENaC subunit affect pH-sensitivity and sodium self-inhibition

To identify molecular determinants that facilitate ENaC inhibition by extracellular  $Na^+$  ions, Kashlan *et al.* (23) previously reported the presence of a putative binding site for  $Na^+$  in the extracellular loop of the  $\alpha$ -subunit in mouse ENaC, which was termed the acidic cleft. Site-directed mutagenesis of several acidic residues within this region altered SSI of mouse  $\alpha\beta\gamma$ -ENaC and in one instance additionally affected sensitivity to extracellular acidification. Hypothesizing the presence of an analogous site of interaction in *Xenopus*  $\delta$ -ENaC, we aimed to determine the effect of mutating key acidic residues within the  $\delta$ -subunit of *Xenopus* ENaC on channel modulation by pH and  $Na^+$ . Fig. 6*a* shows a 3D model of a *Xenopus*  $\delta\beta\gamma$ -ENaC trimer based on the cryo-EM-derived structure of human  $\alpha\beta\gamma$ -ENaC (PDB code 6BQN (7)). The region corresponding to the acidic cleft in mouse  $\alpha$ -ENaC is located at the interface between the  $\beta 2$ - $\alpha 1$  and  $\beta 6$ - $\beta 7$  loops at the top of the  $\delta$ -ENaC extracellular domain (Fig. 6*a*, red area). This region contains three negatively charged aspartates ( $\delta Asp$ -105,  $\delta Asp$ -293, and  $\delta Asp$ -296) that provide potential sites for protonation and potentially contribute to the coordination of  $Na^+$  ions (Fig. 6, *b* and *c*) (24, 25). Within the corresponding structure of *Xenopus*  $\alpha$ -ENaC, two of these aspartates are replaced by a lysine ( $\alpha Lys$ -105) and a glutamate ( $\alpha Glu$ -296), respectively (Fig. 6*c*). In line with previous observations (23), these structural discrepancies may sufficiently alter the  $Na^+$ - and proton-sensitivity of the  $\alpha$ -ENaC acidic cleft. To examine a putative role of the acidic cleft in proton-mediated activation and SSI of *Xenopus*  $\delta\beta\gamma$ -ENaC, we generated mutant channels containing either single ( $\delta_{D105K}$ ,  $\delta_{D293N}$ , and  $\delta_{D296N}$ ), double ( $\delta_{D105K,D296N}$  and  $\delta_{D293N,D296N}$ ), or triple ( $\delta_{D3}$ :  $\delta_{D105K,D293N,D296N}$ ) substitutions of aspartates within this region. The charge-reversing  $\delta_{D105K}$  mutation was chosen, as the presence of a negatively charged  $\delta Asp$ -105 in place of a lysine in  $\alpha$ -ENaC ( $\alpha Lys$ -105) represents the primary difference between both subunits' acidic clefts. Because negatively charged side chains in positions  $\delta Asp$ -293 and  $\delta Asp$ -296 are conserved in the acidic cleft of  $\alpha$ -ENaC, we decided to investigate their impact on pH- and  $Na^+$ -mediated channel regulation through introduction of charge-neutralizing mutations.

The magnitude of acid-induced activation of WT or mutant channels was assayed by successively decreasing extracellular pH from 8.0 to 6.0 in pH 0.2 increments (see Fig. 3). Introduction of single aspartate substitutions within the  $\delta$ -ENaC acidic cleft significantly reduced maximal acid-induced channel activation when compared with WT  $\delta\beta\gamma$ -ENaC (Fig. 7, *a* and *b*, and Table 1). This effect was not cumulative in double-mutant channels, as maximal acid-induced activation of  $\delta_{D105K,D296N}\beta\gamma$  and  $\delta_{D293N,D296N}\beta\gamma$  was not significantly different from that of ENaC containing only single aspartate substitutions. However, mutation of all aspartates in the  $\delta$ -ENaC acidic cleft ( $\delta_{D3}$ ) further decreased the maximal acid-induced channel activation when compared with double-mutant channels (Table 1). Reduction of ENaC activity at alkaline pH was curtailed in all mutant channels except those containing the  $\delta_{D293N}$  mutation (Table 1). The SSI of WT and



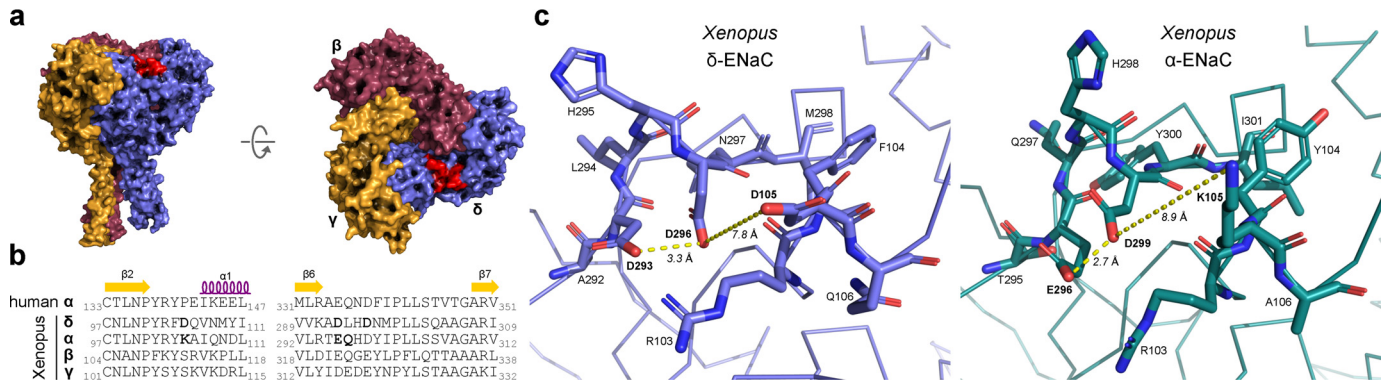


**Figure 6. Comparison of acidic cleft residues in *Xenopus*  $\delta$ - and  $\alpha$ -ENaC subunits.** *a*, structural arrangement of a *Xenopus*  $\delta\beta\gamma$ -ENaC trimer with the position of the  $\delta$ -ENaC acidic cleft highlighted in red. *b*, sequence alignments of human and *Xenopus* ENaC subunits depicting the  $\beta 2$ - $\alpha 1$  and  $\beta 6$ - $\beta 7$  loops that constitute parts of the  $\delta$ -ENaC acidic cleft. **Bold letters** indicate acidic cleft residues that have been mutated in this study. *c*, models of the acidic cleft within *Xenopus*  $\delta$ - and  $\alpha$ -ENaC. Residues in the acidic cleft are shown as stick representations with the rest of the protein chain depicted as ribbon representations. Contacts between residues in the acidic cleft are highlighted with distances shown.

mutant *Xenopus*  $\delta\beta\gamma$ -ENaC was assessed at extracellular  $[\text{Na}^+]$  from 3 to 120 mM as described above. Interestingly, ENaCs containing the  $\delta_{D296N}$  mutation ( $\delta_{D296N}\beta\gamma$ ,  $\delta_{D293N,D296N}\beta\gamma$ , and  $\delta_{D3}\beta\gamma$ ) exhibited a strongly reduced SSI with moderate inhibition of channel activity in the presence of 3 mM  $\text{Na}^+$  ( $\delta_{D296N}\beta\gamma$ ,  $0.23 \pm 0.04$ ) that did not increase with  $[\text{Na}^+]$  ( $\delta_{D296N}\beta\gamma$  SSI at 120 mM  $\text{Na}^+ = 0.18 \pm 0.02$ ,  $n = 16$ ; Fig. 7, *c* and *d*). Although introduction of  $\delta_{D105K}$  or  $\delta_{D293N}$  also decreased maximal SSI compared with WT channels, the considerably reduced effect of these mutations indicates an essential role for the  $\delta$ Asp-296 residue in SSI of *Xenopus*  $\delta\beta\gamma$ -ENaC.

Functional convergence of ENaC regulation by protons and  $\text{Na}^+$  within the acidic cleft was further investigated through assessment of the half-maximal proton-induced activation (pH  $EC_{50}$ ) in the presence of high (90 mM) and low (3 mM)  $[\text{Na}^+]$  (Fig. 7, *e* and *f*). Consistent with the results shown in Fig. 4, *e* and *f*, the pH  $EC_{50}$  of WT  $\delta\beta\gamma$ -ENaC significantly shifted from  $6.93 \pm 0.02$  ( $n = 11$ ) in the presence of 90 mM  $[\text{Na}^+]$  to  $7.49 \pm 0.05$  ( $n = 12$ ;  $p < 0.001$ ) under 3 mM  $[\text{Na}^+]$ . This shift was lost in  $\delta\beta\gamma$ -ENaC containing the single  $\delta_{D296N}$  or triple  $\delta_{D3}$  mutations. Instead, the pH  $EC_{50}$  of channels containing acidic cleft mutations was shifted toward more alkaline values in the presence of 90 mM  $[\text{Na}^+]$  when compared with WT  $\delta\beta\gamma$ -ENaC.

Taken together, these results suggest a contribution of negatively charged residues within the acidic cleft of *Xenopus*  $\delta$ -ENaC to the regulation of channel activity by pH and SSI. Notably, the charge-neutralizing  $\delta_{D296N}$  mutation seems sufficient for almost complete ablation of SSI, while also profoundly decreasing acid-induced ENaC activation. Because substitutions at the  $\delta$ Asp-105 and  $\delta$ Asp-293 positions mimicked the  $\delta_{D296N}$  effect on pH-mediated regulation of *Xenopus*  $\delta\beta\gamma$ -ENaC but induced a less profound reduction of SSI, distinct contributions of these positions to channel regulation by protons and  $\text{Na}^+$  may be hypothesized.

#### The acidic cleft is necessary but not sufficient for enhanced pH-sensitivity of *Xenopus* $\delta\beta\gamma$ -ENaC

To test whether the acidic cleft of  $\delta$ -ENaC is sufficient for enhanced acid-induced ENaC activation, we mutated corresponding residues within *Xenopus*  $\alpha\beta\gamma$ -ENaC. Neither partial ( $\alpha_{K105D}$ ) nor full ( $\alpha_{K105D,E296D,Q297L}$ ) reconstitution of the

$\delta$ -ENaC acidic cleft in the  $\alpha$ -ENaC subunit conveyed an enhanced pH-sensitivity to the channel (Fig. 7*g*), thus deeming the acidic cleft necessary but not sufficient for proton-mediated activation of *Xenopus* ENaC. Previous work on vertebrate ASICs revealed that a segment connecting the first two  $\beta$ -sheets within the proximal part of the channel's ectodomain modifies ASIC-gating kinetics and pH-sensitivity independently of the proton sensor within the acidic pocket (26, 27). Comparison of the corresponding peptide sequence in vertebrate ENaCs revealed that a leucine residue is conserved in the  $\beta 1$ - $\beta 2$  linker of  $\alpha$ -ENaC orthologs, whereas  $\delta$ -ENaC contains a lysine at this position (Fig. 9). Our homology model of *Xenopus*  $\delta$ -ENaC indicates  $\delta$ Lys-89 to be located in the subunit's extracellular loop, where it is oriented toward the  $\beta 9$ -sheet of the  $\delta$ -ENaC palm domain (Fig. 8*a*). Substitution of this lysine by a leucine ( $\delta_{K89L}$ ) significantly shifted the pH dependence of the channel to more acidic values (Fig. 8*b*). Interestingly, baseline currents generated by  $\delta_{K89L}\beta\gamma$ -ENaC were strongly reduced under alkaline to neutral pH conditions, but still susceptible to strong acid-induced activation, leading to an enhanced stimulus-activated character of this mutant channel.

In summary, we have demonstrated that incorporation of the  $\delta$ -subunit confers a pronounced pH-sensitivity to *Xenopus* ENaC, generating acid-activated ion channels. Protons antagonize SSI and induce ENaC activation by increasing channel open probability. Mutational analysis of single aspartates within the  $\delta$ -ENaC acidic cleft suggests a functional convergence of channel regulation by pH and SSI within this region. Although necessary, the presence of an acidic cleft is not sufficient to enhance proton-sensitivity of ENaC. Analogous to vertebrate ASIC1, the  $\beta 1$ - $\beta 2$  linker in ENaC further modifies the apparent pH-sensitivity of *Xenopus*  $\delta\beta\gamma$ -ENaC.

#### Discussion

This study aimed to determine whether functional traits of ancestral proton-activated ion channels are retained in the  $\delta\beta\gamma$ -ENaC isoform of the anuran *X. laevis*. Indeed, our results demonstrate that *Xenopus*  $\delta\beta\gamma$ -ENaC, unlike  $\alpha\beta\gamma$ -ENaC, is profoundly sensitive to changes in the extracellular pH. Extracellular acidification from pH 8.0 to 6.0 resulted in a 7–8-fold increase of amiloride-sensitive transmembrane currents in

## pH-sensitivity of *Xenopus* $\delta$ -ENaC

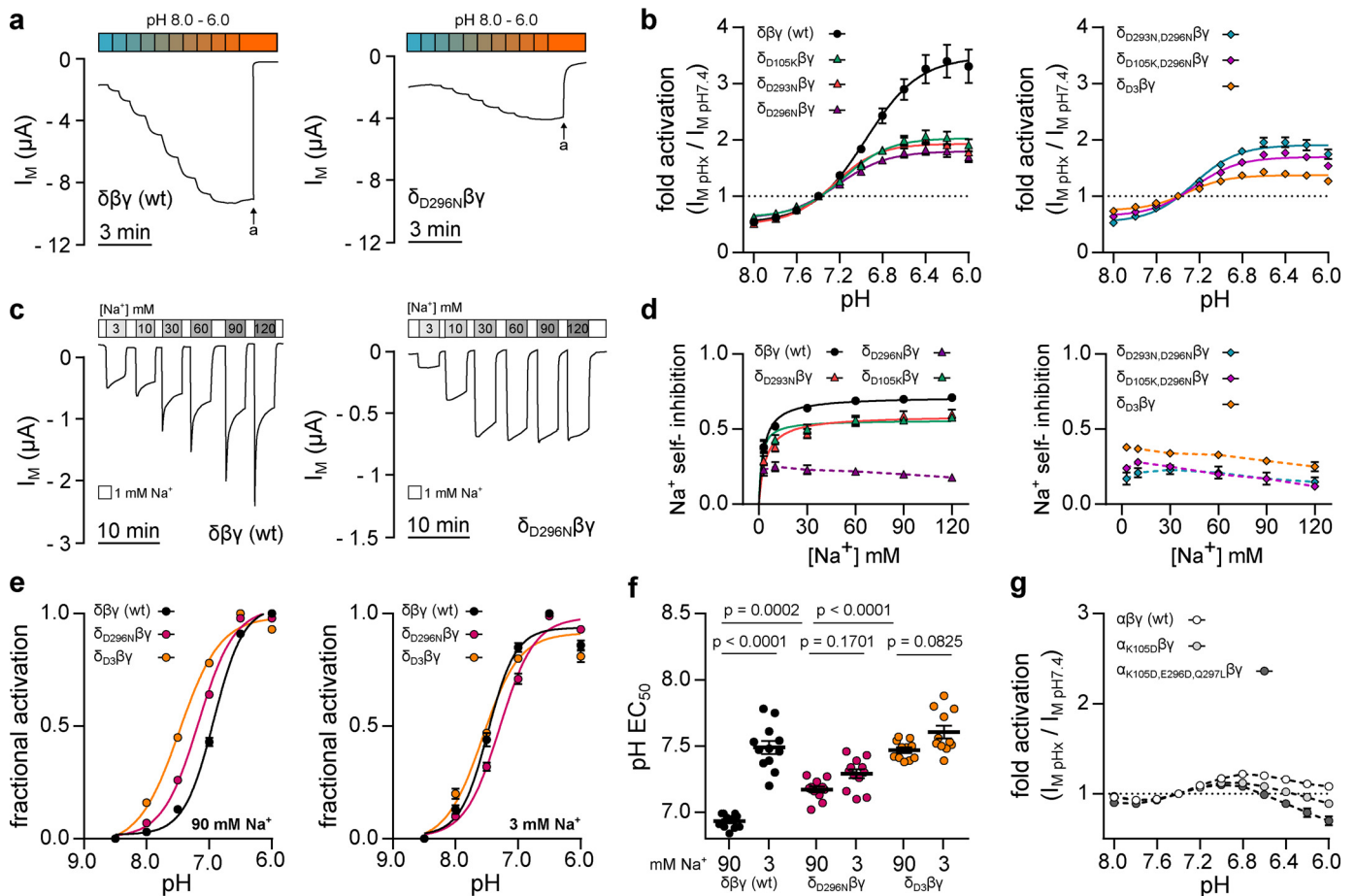


**Figure 7. Three aspartates in the  $\delta$ -ENaC acidic cleft distinctly affect ENaC sensitivity to pH and  $Na^+$ .** *a*, representative  $I_M$  recordings of *Xenopus* oocytes expressing WT  $\delta\beta\gamma$ -ENaC or channels containing a single aspartate to asparagine ( $\delta_{D296N}\beta\gamma$ ) mutation. Channel sensitivity to pH was assessed by a stepwise reduction of extracellular pH from 8.0 to 6.0 (pH 0.2 increments). *b*, pH-dependent activation of  $\delta\beta\gamma$ -ENaC containing none (wt), one ( $\delta_{D105K}\beta\gamma$ ,  $\delta_{D293N}\beta\gamma$ , and  $\delta_{D296N}\beta\gamma$ ), two ( $\delta_{D293N,D296N}\beta\gamma$  and  $\delta_{D105K,D296N}\beta\gamma$ ) or three ( $\delta_{D3}\beta\gamma$ :  $\delta_{D105K,D293N,D296N}\beta\gamma$ ) mutations leading to substitution of single aspartates. Maximum acid-induced channel activation is reduced in ENaC-containing single mutations ( $\delta_{D105K}\beta\gamma$ ,  $\delta_{D293N}\beta\gamma$ , and  $\delta_{D296N}\beta\gamma$ ) when compared with WT  $\delta\beta\gamma$ -ENaC. There is no cumulative effect in channels containing two mutated aspartates, but substitution of three aspartates ( $\delta_{D3}\beta\gamma$ ) further decreases maximum acid-induced activation as well as alkaline channel inhibition (Kruskal-Wallis test,  $p < 0.0001$ ; Dunn's multiple comparisons test). *c*, assessment of SSI at  $[Na^+]$  from 3 to 120 mM in oocytes expressing WT ( $\delta\beta\gamma$ ) or mutant ( $\delta_{D296N}\beta\gamma$ ) ENaC.  $Na^+$  self-inhibition ( $(I_{M, peak} - I_{M, 3 min}) / I_{M, peak}$ ) of WT, single, double, and triple mutant channels. Introduction of  $\delta_{D293N}$  or  $\delta_{D105K}$  moderately decreases maximal SSI when compared with WT  $\delta\beta\gamma$ -ENaC, whereas ENaC containing  $\delta_{D296N}$  has a profoundly reduced SSI irrespective of the extracellular  $[Na^+]$ . Substitution of additional aspartates in double or triple mutant channels does not further decrease ENaC SSI (one-way ANOVA,  $F = 10.26$ ,  $p = 0.0003$ ; Tukey's multiple comparisons test). *d*, proton-sensitivity of  $\delta\beta\gamma$ -ENaC mutants was assessed by determining fractional channel activation ( $(I_{M, x} - I_{M, min}) / \Delta_{max} I_M$ ) resulting from a stepwise reduction of the extracellular pH (pH 8.5–6.0; pH 0.5 increments) in the presence of 90 or 3 mM extracellular  $Na^+$ . *e*, reduction of extracellular  $[Na^+]$  evokes an alkaline-shift of the pH  $EC_{50}$  in WT  $\delta\beta\gamma$ -ENaC but not in channels containing the  $\delta_{D296N}\beta\gamma$  or  $\delta_{D3}\beta\gamma$  mutations. However, in the presence of 90 mM  $Na^+$ , introduction of these mutations shifts the pH  $EC_{50}$  to more alkaline values, when compared with WT ENaC (one-way ANOVA,  $F = 48.02$ ,  $p < 0.0001$ ; Tukey's multiple comparisons test). *f*, pH-sensitivity of *Xenopus*  $\alpha\beta\gamma$ -ENaC ( $n = 11$ ) is not enhanced by partial ( $\alpha_{K105D}\beta\gamma$ ;  $n = 13$ ) or full ( $\alpha_{K105D,E296D,Q297L}\beta\gamma$ ;  $n = 12$ ) reconstitution of the  $\delta$ -ENaC acidic cleft in this subunit. Individual values for pH-mediated regulation and SSI of WT and mutant ENaC (a–d), including statistical analyses, are listed in Table 1.

oocytes expressing *Xenopus*  $\delta\beta\gamma$ -ENaC (Fig. 3). This stimulatory effect of extracellular protons is much stronger compared with *Xenopus*  $\alpha\beta\gamma$ -ENaC (Fig. 3), human ENaC orthologs (Fig. 3) (14), or rodent ENaCs (23, 28). The reversibility and relatively fast time course of acid-induced ENaC activation suggest that protons interfere with ENaC gating, rather than altering membrane abundance of the channel. This is in line with previous studies that either demonstrated a decreased pH-sensitivity of ENaCs containing gating-mutations (14, 29) or reported a direct influence of protons on ENaC  $P_o$  (30, 31). Consistently, cell-attached patch-clamp recordings presented in this study indicate an inverse correlation between pH and ENaC  $P_o$  (Fig. 2b). Previous studies reported a significant inhibition of rat  $\alpha\beta\gamma$ -ENaC by cytoplasmic acidification (31, 32),

but changes in the extracellular pH within a range that was employed in our study have a slow and marginal effect on the cytoplasmic pH of *Xenopus* oocytes (33, 34). Although we cannot completely exclude a contribution of changes in the intracellular pH to modulation of *Xenopus*  $\delta\beta\gamma$ -ENaC activity, our results suggest that channel gating is predominantly affected by extracellular protons.

Previous studies have suggested that acid-induced ENaC activation involves a relief from SSI, which describes an allosteric reduction of ENaC  $P_o$  due to the binding of  $Na^+$  to the extracellular domain of the channel (20, 23). Collier *et al.* (2009) demonstrated that extracellular acidification (pH 8.5–6.5) reduces the magnitude but not the  $Na^+$  affinity of SSI in human  $\alpha\beta\gamma$ -ENaC, thereby suggesting that protons trigger conforma-



**Table 1**  
**pH-mediated regulation and Na<sup>+</sup> self-inhibition of  $\delta$ -ENaC acidic cleft mutants**

Individual values for pH-mediated regulation and Na<sup>+</sup> self-inhibition of *Xenopus*  $\delta\beta\gamma$ -ENaC containing aspartate substitutions in the  $\delta$ -ENaC acidic cleft derived from recordings as presented in Fig. 7, a–d. Values for maximal activation and minimal activity in the “pH-mediated channel activation” columns are based on individual sigmoidal dose-response functions. Statistical evaluation of these data was performed as follows: maximal activation (Kruskal-Wallis test,  $p < 0.0001$ ; Dunn’s multiple comparisons test); minimal activity (one-way ANOVA,  $F = 12.11$ ,  $p < 0.0001$ ; Tukey’s multiple comparisons test). Values for  $V_{\max}$  and  $K_m$  in the “Na<sup>+</sup> self-inhibition” columns are derived from individual Michaelis-Menten plots where applicable. Statistical evaluation of the corresponding data was performed as follows:  $V_{\max}$  (Kruskal-Wallis test,  $p < 0.0001$ ; Dunn’s multiple comparisons test);  $K_m$  (Kruskal-Wallis test,  $p = 0.061$ ; Dunn’s multiple comparisons test). All values represent mean  $\pm$  S.E.

	pH-mediated channel activation			Na <sup>+</sup> self-inhibition		
	Maximal activation	Minimal activity	<i>n</i>	$V_{\max}$	$K_m$ (mM Na <sup>+</sup> )	<i>n</i>
$\delta\beta\gamma$ -ENaC	3.48 $\pm$ 0.31 <sup>a</sup>	0.5 $\pm$ 0.03 <sup>a</sup>	22	0.72 $\pm$ 0.01	3.8 $\pm$ 0.7	16
$\delta_{D105K}\beta\gamma$	2.04 $\pm$ 0.11 <sup>a,b</sup>	0.62 $\pm$ 0.02 <sup>b</sup>	14	0.57 $\pm$ 0.03 <sup>b</sup>	2.7 $\pm$ 1.2	9
$\delta_{D293N}\beta\gamma$	1.94 $\pm$ 0.07 <sup>a,b</sup>	0.49 $\pm$ 0.03 <sup>a</sup>	14	0.62 $\pm$ 0.03 <sup>b</sup>	8.9 $\pm$ 3.6	16
$\delta_{D296N}\beta\gamma$	1.81 $\pm$ 0.10 <sup>b</sup>	0.60 $\pm$ 0.02 <sup>a,b</sup>	16			12
$\delta_{D293N,D296N}\beta\gamma$	1.92 $\pm$ 0.09 <sup>a,b</sup>	0.54 $\pm$ 0.02 <sup>a</sup>	19			15
$\delta_{D105K,D296N}\beta\gamma$	1.7 $\pm$ 0.04 <sup>a,b</sup>	0.65 $\pm$ 0.02 <sup>b</sup>	17			11
$\delta_{D105K,D293N,D296N}\beta\gamma$	1.38 $\pm$ 0.04 <sup>b</sup>	0.74 $\pm$ 0.03 <sup>b</sup>	12			10

<sup>a</sup>  $p < 0.05$  when compared with  $\delta_{D105K,D293N,D296N}\beta\gamma$ -ENaC in the respective column.

<sup>b</sup>  $p < 0.05$  when compared with wildtype  $\delta\beta\gamma$ -ENaC in the respective column.

tional changes that affect ENaC gating downstream of Na<sup>+</sup> binding. The results we presented in this study indicate a similar functional interdependence between pH and SSI in *Xenopus*  $\delta\beta\gamma$ -ENaC, because extracellular acidification (pH 8.0–6.0) also reduced the  $V_{\max}$  of SSI in *Xenopus*  $\delta\beta\gamma$ -ENaC in a dose-dependent manner (Fig. 5). However, we observed an increased potency of acidic pH in curtailing SSI of this amphibian ENaC isoform, which is potentially caused by a proton-mediated antagonism of Na<sup>+</sup> binding at a conserved Na<sup>+</sup> coordination site within an acidic cleft of the  $\delta$ -ENaC ectodomain.

Additional evidence for functional convergence of ENaC regulation by pH and SSI comes from mutations within the  $\delta$ -ENaC acidic cleft, which decreased both acid-induced channel activation as well as ENaC inhibition through SSI (Fig. 7). This is consistent with previous findings that demonstrated a contribution of conserved negatively charged residues in the acidic cleft of mouse  $\alpha$ -ENaC to both SSI and pH (23). The authors suggested the acidic cleft as a potential Na<sup>+</sup>-binding site that initiates SSI and proposed that protonation of a central aspartate (Asp-296 in *Xenopus*  $\delta$ -ENaC) at acidic pH would obstruct Na<sup>+</sup> coordination. Consistent with this hypothesis, the  $\delta_{D296N}$  mutation led to a full disruption of SSI in *Xenopus*  $\delta\beta\gamma$ -ENaC, while also partially impeding acid-induced channel activation (Fig. 7). A model involving a proton-mediated antagonism of Na<sup>+</sup> binding, which would contribute to subsequent channel activation by disruption of SSI, is consistent with the observed shift in half-maximal proton-induced activation of  $\delta\beta\gamma$ -ENaC due to a reduction of the extracellular [Na<sup>+</sup>] (Fig. 4, e and f) as well as  $\delta$ -ENaC acidic cleft mutations that mimic this effect (Fig. 7, e and f). Furthermore, we observed a decrease in the apparent Na<sup>+</sup> affinity of SSI as a result from extracellular acidification (Fig. 5). It thus seems reasonable to propose that protonation of acidic residues within the  $\delta$ -ENaC acidic cleft shifts the Na<sup>+</sup>-binding equilibrium of this coordination site and thereby impedes initiation of SSI. Substitutions of nearby located aspartates in the  $\delta$ -ENaC acidic cleft ( $\delta_{D105K}$  and  $\delta_{D293N}$ ), however, did not lead to a full ablation of SSI, whereas acid-induced channel activation was reduced to a similar extent as observed with the  $\delta_{D296N}$  mutation (Fig. 7). This accentuates a central role for the negative charge of the  $\delta$ Asp-296 moiety in ENaC SSI, potentially involving coordination of Na<sup>+</sup> at this position. Interestingly, as indicated in Fig. 9, the negative

charge present in *Xenopus*  $\delta$ Asp-296 is strongly conserved throughout the  $\alpha$ -ENaC lineage as well as in other members of the degenerin/ENaC family (7, 35), whereas it is lost in most mammalian  $\delta$ -ENaC orthologs. Although conservation of this residue would imply a central role in channel functionality, its presence does not seem to correlate with an increased pH-sensitivity or SSI of ENaC. However, we found that introduction of the neighboring  $\delta_{D105K}$  or  $\delta_{D293N}$  mutations in *Xenopus*  $\delta$ -ENaC led to a small but significant reduction in the magnitude of ENaC SSI while also significantly reducing proton-induced channel activation. Thus, it may be speculated that the proximate molecular environment of  $\delta$ Asp-296 additionally modifies Na<sup>+</sup> coordination within the acidic cleft, allowing for modification of Na<sup>+</sup>- and pH-sensitivity without altering basic channel functionality. Consistently, the structural similarities between the acidic cleft of *Xenopus*  $\delta$ -ENaC and  $\alpha$ -ENaC subunits (Fig. 6; also see Fig. 9) suggest that subtle amino acid alterations within this extracellular region may have profound effects on the channel’s pH-sensitivity. This is interesting from an evolutionary perspective, because mutations within the acidic cleft might have the potential to transform a proton-stimulated ENaC ancestor into a less proton-sensitive and rather constitutively active channel. Indeed, it was recently highlighted that functional diversification within the degenerin/ENaC protein family is associated with a high variability in the extracellular regions contributing to the formation of the acidic cleft, including the knuckle and finger domains as well as the  $\beta 6$ – $\beta 7$  loop (2). Three acidic residues within that region are conserved in  $\alpha$ -like ENaC in lamprey as well as  $\delta$ -ENaC in amphibians and reptiles, whereas the number of acidic residues decreases within the mammalian  $\delta$ -ENaC lineage (Fig. 9). Human  $\delta\beta\gamma$ -ENaCs have a largely reduced SSI (36) and lack strong pH-sensitivity (Fig. 3), suggesting a potential correlation between altered acidic cleft structure and constitutive-ENaC activity within the  $\delta$ -ENaC lineage. It is, however, unclear whether the altered structure of the acidic cleft in mammals caused a reduction in SSI or the cleft mutated as a result of functional uncoupling from gating mechanisms. We also note that proton-sensitivity of *Xenopus*  $\delta\beta\gamma$ -ENaC does not necessarily represent a functional trait that was retained during channel evolution but may have developed secondarily in the secondarily aquatic, pipid frog (37). Future studies might focus on

## pH-sensitivity of *Xenopus* $\delta$ -ENaC

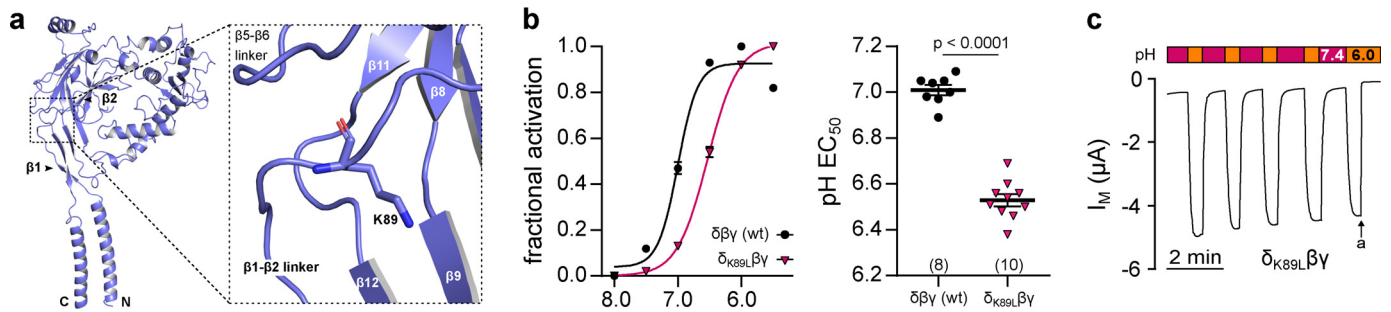




















**Figure 8. Proton sensitivity of *Xenopus*  $\delta\beta\gamma$ -ENaC is further modulated by a lysine in the  $\delta$ -ENaC  $\beta$ 1– $\beta$ 2 linker.** *a*, homology model of the *Xenopus*  $\delta$ -ENaC subunit indicating the location of  $\delta$ Lys-89 in the linker region between the  $\beta$ 1 and  $\beta$ 2 sheets in the palm domain. *b*, fractional channel activation ( $(I_{M,x} - I_{M,min})/\Delta_{max} I_M$ ) resulting from a stepwise reduction of the extracellular pH (pH 8.0–5.5; pH 0.5 increments) in WT and  $\delta_{K89L}\beta\gamma$ -ENaC. Introduction of the  $\delta_{K89L}$  mutation leads to a significant acidic-shift of the channel's  $pH EC_{50}$  (Student's unpaired *t* test). *c*, representative  $I_M$  recording of an oocyte expressing  $\delta_{K89L}\beta\gamma$ -ENaC. Macroscopic currents mediated by mutant channels display "stimulus-activated" characteristics as they are low at neutral pH 7.4 and reversibly increased by extracellular acidification (pH 6.0, 30 s; a = amiloride, 100  $\mu$ M).

comparing pH-mediated regulation of ENaC orthologs from species representing early tetrapod ancestors to attain a better understanding of this conundrum. In contrast to  $\delta$ -ENaC, proteolytic processing has exclusively been established in the  $\alpha$ -ENaC lineage, as represented by the presence of two furin cleavage sites in subunit orthologs from terrestrial tetrapods (Fig. 9) (38). Furin cleavage activates ENaC by uncoupling the channel from SSI (19). This might provide a potential explanation for the strong conservation of the acidic cleft structure and residual pH-sensitivity in the  $\alpha$ -ENaC lineage (Fig. 9).

The recently resolved structure of human  $\alpha\beta\gamma$ -ENaC identified extensive contacts between the knuckle and finger domains of neighboring subunits, forming a collar of inter-subunit interactions at the top of the extracellular loop (7). The  $\alpha$ -helices from the knuckle ( $\alpha$ 6) and the finger domains ( $\alpha$ 1 and  $\alpha$ 2) of human ENaC were shown to enclose the  $\beta$ 6– $\beta$ 7 loop that has been proposed to form part of the acidic cleft in mouse  $\alpha$ -ENaC (23) as well as *Xenopus*  $\delta$ -ENaC (Fig. 6). The homology model of *Xenopus*  $\delta\beta\gamma$ -ENaC presented in this study indicates the  $\beta$ 6– $\beta$ 7 loops of individual subunits to be located between the  $\beta$ 2– $\alpha$ 1 loop preceding the finger domain and the  $\alpha$ 6– $\beta$ 11 loop of the knuckle domain within the same subunit, generating individual intra-subunit conjunctions. Conformational changes due to the coordination of  $Na^+$  in the  $\delta$ -ENaC acidic cleft may therefore be transmitted by means of the knuckle–finger collar to drive structural reorganizations that eventually lead to the adoption of a low  $P_o$  ENaC-gating mode. Conversely, protonation of the acidic cleft could oppose  $Na^+$  coordination at this site and thereby shift the channel's gating equilibrium toward a high  $P_o$  state. Although a precise mechanistic interpretation of how the acidic cleft contributes to regulation of *Xenopus*  $\delta\beta\gamma$ -ENaC gating by pH and SSI may not be feasible based on the present results, they clearly demonstrate that both modulatory factors converge within the acidic cleft where they likely interact in a competitive manner.

Additionally, protons likely modulate conformational changes, which would induce a transition into a low  $P_o$ -gating mode, downstream from the binding of extracellular  $Na^+$ . The presence of a component in acid-induced activation of  $\delta\beta\gamma$ -ENaC that is independent of  $Na^+$  coordination at the acidic cleft is indicated by the residual pH-sensitivity of  $\delta_{D296N}\beta\gamma$  mutant channels, which do not exhibit SSI (Fig. 7). Previous studies by Snyder and co-workers (14, 28) have identified a crucial role of

titratable residues within the  $\beta$ - and  $\gamma$ -ENaC subunits in facilitating acid-induced activation of human  $\alpha\beta\gamma$ -ENaC. Further investigations by the same group (39) convincingly demonstrated that key pH-sensitive residues located at the interfaces between adjacent channel subunits affect ENaC gating by altering intersubunit distances through electrostatic interactions. The subunit composition of *Xenopus* ENaC thus may alter pH-sensitivity, not only by introduction of the  $\delta$ -ENaC acidic cleft but also through the formation of intersubunit interactions in lower parts of the channel's extracellular loop. pH-sensitive residues in human  $\alpha\beta\gamma$  ENaC have been proposed to facilitate acid-induced channel activation through interactions with the  $\beta$ 1– $\beta$ 2 linker in the lower palm domain of adjacent subunits (39). This is in good agreement with our results suggesting that modulatory sites distal to the acidic cleft, such as the  $\delta$ -ENaC  $\beta$ 1– $\beta$ 2 linker, affect proton-induced activation of *Xenopus*  $\delta\beta\gamma$ -ENaC (Fig. 8). These observations also suggest interesting similarities to the molecular mechanisms determining pH-sensitivity of ASICs. For example, mutations in the  $\beta$ 1– $\beta$ 2 linker conveyed pH-sensitivity to lamprey ASIC1 (26), largely increased macroscopic and acid-induced current amplitudes of elephant shark ASIC1 (27), and decreased the velocity of *Xenopus* ASIC1.1 activation. Analogous to the proposed evolutionary adaptation of pH-sensitivity in ASICs from early diverging vertebrates (27), structural modifications in the  $\beta$ 1– $\beta$ 2 linker could have enabled diversification of proton-sensitivity in ENaC isoforms due to changes within the palm domain and independently of the structure of the acidic cleft. Furthermore, pH-sensitivity of mouse ASIC1a was reported to be affected by mutations of Lys-211, which links the palm and thumb domains of neighboring subunits (16). Conservation of the positive charge at the corresponding position in *Xenopus*  $\delta$ -ENaC ( $\delta$ Arg-279) could additionally account for pH-sensitivity of this channel isoform, whereas its absence in the  $\alpha$ -ENaC subunit ( $\alpha$ Met-282) might prevent acid-induced channel activation. Taken together, we propose that extracellular acidification activates *Xenopus*  $\delta\beta\gamma$ -ENaC through modulation of SSI by means of at least two distinct mechanisms. Protonation of acidic residues within the  $\delta$ -ENaC acidic cleft likely shifts the  $Na^+$ -binding equilibrium of a  $Na^+$  coordination site and thus impedes initiation of SSI. Additionally, protons potentially interfere with conformational changes, which would induce the transi-

		$\alpha$ -like					$\delta$ -ENaC				
		Acidic cleft			Furin		Acidic cleft			Furin	
		$\beta 1$ - $\beta 2$	$\beta 2$ - $\alpha 1$	$\beta 6$ - $\beta 7$	1st	2nd	$\beta 1$ - $\beta 2$	$\beta 2$ - $\alpha 1$	$\beta 6$ - $\beta 7$	1st	2nd
	<i>E. burgeri</i>	QST	ESE	DRHN	X	X					
	<i>P. marinus</i>	QST	YEV	EQND	X	X					
		$\alpha$ -ENaC					$\delta$ -ENaC				
		Acidic cleft			Furin		Acidic cleft			Furin	
		$\beta 1$ - $\beta 2$	$\beta 2$ - $\alpha 1$	$\beta 6$ - $\beta 7$	1st	2nd	$\beta 1$ - $\beta 2$	$\beta 2$ - $\alpha 1$	$\beta 6$ - $\beta 7$	1st	2nd
	<i>L. chalumnae</i>	KLL	YKE	EQND	✓	X	PKI	YTQ	KQED	X	X
	<i>P. annectens</i>	KLV	YNA	EQND	X	X					
	<i>N. forsteri</i>	KLI	YNV	EQND	X	X					
	<i>X. laevis</i>	KLP	YKA	EQHD	✓	✓	GKI	FDQ	DLHD	X	X
	<i>N. parkeri</i>	RLI	YHS	EQND	✓	✓	KSN	FDQ	DQHD	X	X
	<i>P. sinensis</i>	KLT	YSA	EQND	✓	✓	PKM	FDL	EHND	X	X
	<i>P. bivittatus</i>	RLT	YSA	EQND	✓	✓	PKM	ISP	EQKD	X	X
	<i>A. mississippiensis</i>	RLT	YSA	EQND	✓	✓	PKM	FAT	EQKD	X	X
	<i>G. gallus</i>	RLT	YSA	EQND	✓	✓	PKM	FDL	EQKD	X	X
	<i>O. anatinus</i>	KLV	YSA	EQKD	✓	✓	PKM	PPL	EQNK	✓	✓
	<i>O. aries</i>	KLI	YKE	EQND	✓	✓	RKL	PHL	EQQD	X	X
	<i>P. troglodytes</i>	KLV	YPE	EQND	✓	✓	RKL	PSP	EQQP	X	✓
	<i>H. sapiens</i>	KLV	YPE	EQND	✓	✓	RKL	PSP	EQQP	X	✓
	<i>C. porcellus</i>	KLV	YKE	EQND	✓	✓	RKL	PGS	EPRV	X	X
	<i>H. glaber</i>	KLV	YKE	EQND	✓	X	SKI	PRA	QTQV	✓	X
	<i>R. norvegicus</i>	KLV	YTE	EQND	✓	✓					

**Figure 9. Conservation of motifs involved in pH-sensitivity and proteolytic maturation of  $\alpha$ - and  $\delta$ -ENaC orthologs.** Multiple sequence alignment inferred from amino acid sequences of  $\alpha$ - and  $\delta$ -ENaC orthologs (Table S1) showing sites involved in proton-mediated activation of *X. laevis*  $\delta\beta\gamma$ -ENaC that have been identified in this study ( $\beta 1$ - $\beta 2$ ,  $\beta 2$ - $\alpha 1$ , and  $\beta 1$ - $\beta 2$  linker). Note that only one  $\alpha$ -like subunit ortholog has been identified in hagfish *Eptatretus burgeri* and lamprey *Petromyzon marinus*, which therefore are displayed in a separate group. Rats do not have a functional gene for  $\delta$ -ENaC. Colored backgrounds illustrate the presence of residues with hydrophobic (blue) or polar (red) side chains in the  $\beta 1$ - $\beta 2$  linker or negatively-charged residues (yellow) in the acidic cleft. The Asp-296 position, which is essential for  $\text{Na}^+$  coordination in *Xenopus*  $\delta\beta\gamma$ -ENaC, is highlighted in red. Conservation of the minimal consensus sequence for proteolytic maturation of ENaC subunits by furin (sequence RXXR) is indicated by green check marks, and red crosses represent the absence of this consensus sequence. Gray checkmarks indicate the presence of an RXXR motif dislocated from the conserved location of the respective furin cleavage site.

tion into a low  $P_o$  gating mode resulting from the binding of extracellular  $\text{Na}^+$ .

Finally, the results presented in this study suggest a putative physiological role of ENaCs containing the  $\delta$ -subunit. In adult *X. laevis*, we found  $\delta$ -ENaC mRNA exclusively in tissue samples from the urogenital tract, including the kidneys, urinary bladder, and cloaca but not in the skin (18). The presence of functional  $\delta\beta\gamma$ -ENaC channels in the apical membrane of epithelial cells within those organs could indicate a coupling of transepithelial  $\text{Na}^+$  absorption to urinary pH. Interestingly, luminal acidification has been shown to stimulate  $\text{Na}^+$  absorption across the toad urinary bladder (40), whereas  $\text{Na}^+$  absorption across the skin was unaffected (41). Indeed, urinary acidification has been observed along the distal mesonephric tubules and the urinary bladder of multiple amphibian and reptile species (42). In the urinary bladder of *Bufo marinus*, mucosal proton secretion was found to be partially associated with an amiloride-sensitive  $\text{Na}^+$  absorption across the bladder epithelium, suggesting a reciprocal coupling between these ion transport mechanisms (43) that might resemble proton-coupled  $\text{Na}^+$  absorption in ionocytes of freshwater fish. Previous work

by Balinsky and Baldwin (44) reported that the urinary pH in *X. laevis* is alkaline (pH 8.0), which might result from ammonotelic nitrogen excretion in this species. Based on our study, this would suggest  $\delta\beta\gamma$ -ENaC activity to be generally low. We have previously shown that currents generated by  $\delta\beta\gamma$ -ENaC are consistently larger than those generated by  $\alpha\beta\gamma$ -ENaC (18), suggesting that ENaCs containing the  $\delta$ -subunit might play a role under conditions where maximum  $\text{Na}^+$  absorption is necessary. *X. laevis* can survive droughts by aestivation, a physiological state where the animals absorb water via the urinary bladder. Nitrogen excretion switches from ammonotelia to ureotelia under aestivation, which might trigger changes in urinary pH. Indeed, McBean and Goldstein (45) reported a reduction in urine flow as well as an increase of plasma  $\text{Na}^+$  levels preventing dehydration of *X. laevis* in an hyperosmotic environment. Similar physiological responses due to salt stress have been observed the aestivating toad *Scaphiopus couchi* (46) and the semiaquatic *B. marinus* (47). However, because the cellular localization of  $\delta\beta\gamma$ -ENaC in the urogenital tract is still unknown, further exploration is warranted to dissect the precise physiological role of this ENaC isoform under such conditions.

In summary, we have demonstrated that *X. laevis*  $\delta\beta\gamma$ -ENaC is a profoundly pH-sensitive ion channel. Proton-sensitivity is partially provided by an extracellular acidic cleft, where protonation of acidic residues is coupled to SSI. These characteristics, together with the evolutionary variability of this extracellular region, suggest that  $\delta$ -ENaC might have evolved from a stimulated-activated ancestor that was uncoupled from proton-sensitivity during the evolution of tetrapod vertebrates.

## Experimental procedures

### Synthesis of cRNA

Constructs encoding full-length human or *X. laevis*  $\delta$ - $\alpha$ - $\beta$ - and  $\gamma$ -ENaC were present in the pTNT expression vector (Promega, Mannheim, Germany). Site-directed mutagenesis (primers listed in Table 2) was performed using the QuikChange Lightning kit (Agilent Technologies, Waldbronn, Germany) according to the manufacturer's instructions. Successful mutagenesis was verified by sequencing (SeqLab, Goettingen, Germany). Constructs were linearized with BamHI ( $\delta$ - and  $\alpha$ -ENaC) or NaeI ( $\gamma$ -ENaC, both enzymes purchased from Promega). Plasmids containing  $\beta$ -ENaC were not linearized due to the presence of BamHI and NaeI restriction sites in the coding sequence. Synthesis of m<sup>7</sup>G-capped cRNA was performed using the T7 RNA polymerase system (RiboMAX large scale RNA production system, Promega) according to the manufacturer's protocol. cRNAs were diluted in diethylpyrocarbonate-treated H<sub>2</sub>O to a final concentration of 10 ng/ $\mu$ l per subunit for two-electrode voltage-clamp (TEVC) recordings and 20 ng/ $\mu$ l for patch-clamp recordings.

### Expression in *Xenopus* oocytes

Stage V/VI oocytes were isolated from adult frogs as described previously (18). Animals were anesthetized in 0.2% MS-222/H<sub>2</sub>O (Pharmaq, New Hampshire, UK) at pH 6.0 for 15 min prior to euthanasia by decapitation and sounding of the spinal cord. The methods used to humanely euthanize the ani-



**Table 2**

**Site-directed mutagenesis primer sequences**

Single nucleotide exchanges for site-directed mutagenesis are highlighted in underlined, bold letters. Generation of constructs containing single amino acid substitutions ( $\delta_{D293N}$ ,  $\delta_{D296N}$ ,  $\delta_{D105K}$ ,  $\delta_{K89L}$  and  $\alpha_{K105D}$ ) as well as the  $\delta_{D293N,D296N}$  double mutant was achieved using wildtype  $\delta$ - or  $\alpha$ -ENaC constructs. The  $\delta_{D105K}$  primers were employed in combination with constructs encoding  $\delta_{D296N}$  or  $\delta_{D293N,D296N}$ -ENaC for generation of  $\delta_{D105K,D296N}$  and  $\delta_{D105K,D293N,D296N}$ -ENaC respectively. Primers introducing the  $\alpha_{K105D}$  mutation were used in combination with constructs containing the  $\alpha_{E296D,Q297L}$  double mutation to create  $\alpha_{K105D,E296D,Q297L}$  triple mutants.

Primer		Primer sequence (5'–3')
$\delta_{D293N}$	Forward	GGCATGTTGTCATGAAGAT <b>T</b> AGCCTTCACAACCATAGAC
	Reverse	GTCTATGGTTGTGAAGGCT <b>A</b> ATCTTCATGACAACATGCC
$\delta_{D296N}$	Forward	GGAGAGGCATGTTGT <b>T</b> ATGAAGATCAGCCTTCACA
	Reverse	TGTGAAGGCTGATCTTCAT <b>A</b> ACAACATGCCTCTCC
$\delta_{D105K}$	Forward	GAGCTGATTAATACATATTAACCT <b>GCTT</b> AAATCTGTAGGGGTTAGATTGCAAAT
	Reverse	ATTTGCAATCTGAACCCCTACAGATTT <b>AAG</b> CAAGTTAATATGTATATTAATCAGCTC
$\delta_{D293N,D296N}$	Forward	GGCATGTTGTT <b>T</b> ATGAAGAT <b>T</b> AGCCTTCACAACCATAGAC
	Reverse	GTCTATGGTTGTGAAGGCT <b>A</b> ATCTTCAT <b>A</b> ACAACATGCC
$\delta_{K89L}$	Forward	GGTCACAGCTGGAAATATT <b>AAG</b> CCCTTTGACTGCAAGCCT
	Reverse	AGGCTTGCAGTCAAAGGGC <b>TT</b> AATATTTCCAGCTGTGACC
$\alpha_{K105D}$	Forward	GCAGATCATCTGAATCGC <b>AT</b> CGTACCTGTACGGGTTTAAG
	Reverse	CTTAAACCCGTACAGGTAC <b>GAT</b> GCGGATTCAGAATGATCTGC
$\alpha_{E296D,Q297L}$	Forward	GGAATGTAATCATGC <b>ACAT</b> CAGTCCGAAGGACAAGGGTTAG
	Reverse	CTAACCCCTTGCTCTCGGACTGA <b>TCT</b> GCATGATTACATTC

imals were consistent with the recommendations of the AVMA Guidelines for the Euthanasia of Animals. All procedures and experimental protocols were approved by the Animal Welfare Officer of the University of Giessen (Registration No.: M\_478/M\_549/M\_649) as well as the Animal Welfare and Ethical Review Body at Newcastle University (Project ID No: ID 630). The animal housing facility (Giessen, Germany) was licensed by local authorities (Az: FD 62-§11 JLU Tierphysiologie). For some experiments, oocytes were purchased from the European *Xenopus* Resource Centre (Portsmouth, UK) or Ecocyte Bioscience (Castrop-Rauxel, Germany). Oocytes were kept in a culture of oocyte Ringer's solution (CulORS, in mM: 90 NaCl, 1 KCl, 2 CaCl<sub>2</sub>, 5 HEPES, 2.5 sodium pyruvate, 0.06 penicillin G, and 0.02 streptomycin sulfate at pH 7.4) prior to injection with 32 nl of cRNA. Cells were incubated at 16 °C in a low-sodium CulORS (in mM: 10 NaCl, 80 *N*-methyl-D-glucamine (NMDG), 1 KCl, 2 CaCl<sub>2</sub>, 5 HEPES, 2.5 sodium pyruvate, 0.06 penicillin G, and 0.02 streptomycin sulfate at pH 7.4) for 1–2 days for two-electrode voltage-clamp measurements or 2–7 days for patch-clamp recordings.

**Electrophysiological recordings**

TEVC and cell-attached patch-clamp recordings were essentially performed as described previously (18). In brief, TEVC recordings of oocyte whole-cell transmembrane currents ( $I_M$ ) were conducted using a Turbo Tec-03X amplifier (NPI, Tamm, Germany) at a holding potential of –60 mV. Current signals were low-pass filtered at 1 kHz and recorded with a strip-chart recorder. If not stated otherwise, oocytes were perfused with ORS (in mM: 90 NaCl, 1 KCl, 2 CaCl<sub>2</sub>, 5 HEPES) through a gravity-driven system at a speed of 10 ml/min. Sodium was substituted with equimolar amounts of NMDG in ORS containing differing sodium concentrations. Adjustment of pH was achieved with HCl and NaOH. NMDG was used for alkaline titration of ORS containing defined Na<sup>+</sup> concentrations. The ENaC inhibitor amiloride (100  $\mu$ M; Sigma-Aldrich, Taufkirchen, Germany) was employed to identify ENaC-mediated current fractions ( $\Delta I_{ami}$ ).

For patch-clamp experiments, mechanically devitellinized oocytes were placed in a recording chamber containing bath solution (in mM: 145 KCl, 1.8 CaCl<sub>2</sub>, 10 HEPES, 2 MgCl<sub>2</sub>, and 5.5 glucose at pH 7.4). Patch pipettes (6–9 megohm resistance) were pulled from borosilicate glass capillaries, heat-polished, and filled with pipette solution (in mM: 145 NaCl, 1.8 CaCl<sub>2</sub>, 10 HEPES, 2 MgCl<sub>2</sub> and 5.5 glucose). The pH of the pipette solution was adjusted using HCl and NaOH. Current signals were amplified using an LM-PC patch-clamp amplifier (List-Medical, Darmstadt, Germany), low-pass filtered at 100 Hz (Frequency Devices, Haverhill, IL), and recorded at 2 kHz with Axon Clampex software (Axon Instruments, Foster City, CA) using an Axon 1200 interface. Single-channel analysis was performed with Clampfit version 10.7 (Axon Instruments). The amount of channels in each recording was stochastically estimated by comparing the number of visible channels with a theoretical amount derived from binomial distribution as described previously (21). All electrophysiological recordings were performed at room temperature.

**Homology modeling**

Homology modeling of *Xenopus* ENaC isoforms was performed using the I-Tasser web server (48) and PyMol (The PyMOL Molecular Graphics System, Version 2.0, Schrödinger, LLC) to generate the heterotrimeric complexes based on the cryo-EM–derived structure of human  $\alpha\beta\gamma$ -ENaC (PDB code 6BQN (7)). Sequence alignments were generated employing the Clustal Omega online tool (49).

**Vertebrate ENaC sequence analysis**

Protein sequences of different vertebrate  $\alpha$ - and  $\delta$ -ENaC orthologs were collected from the UniProt and NCBI Protein databases. Because many protein sequences are *in silico* translation products from genomic DNA of sequencing efforts from different animals that have yet not been validated by cDNA cloning, verification of available sequence information was required. To verify, or complete, a coding DNA sequence, the genomic sequence information was compared with known cod-

ing sequences from other species such as human or *Xenopus*. If available, genomic sequence information was retrieved from the linked sources of the respective protein sequences (Table S1). In other cases, sequence information from closely related species was submitted to BLASTN (NCBI) with default parameters for megablast/blast algorithms choosing the database for whole-genome shotgun contigs and specifying the respective organism or family. Depending on the size of the output sequence, all sequences were immediately or iteratively compared with confirmed exon sequences using MultAlin (<http://multalin.toulouse.inra.fr/multalin/>)<sup>3</sup> (51) with parameters set for DNA alignment. The comparison included determination of the exon boundaries and the quality of the splice donor and acceptor sites, exon length (as a consistent feature across various species and isoforms), as well as potential Kozak consensus sequences for the translational start. The verified or completed cDNA sequence information was finally translated into the respective amino acid sequence (<https://web.expasy.org/translate/>;<sup>3</sup> Table S1). Generation of sequence alignments using the ClustalW algorithm was achieved employing the Mega X suite.

### Data analysis

Data are presented in column scatter plots or  $x$ - $y$  graphs with lines/symbols and error bars representing mean  $\pm$  S.E. Oocytes for each experiment were derived from at least three different donors, and the number of individual experiments ( $n$ ) is noted in parentheses. Statistical analyses were performed using GraphPad Prism version 7 (GraphPad Software Inc., La Jolla, CA). Gaussian distribution of individual data were assessed with the D'Agostino and Pearson omnibus normality test. Multiple groups were compared by one-way ANOVA followed by a post hoc Tukey's multiple-comparison test (two-tailed) for normally distributed data or a Kruskal-Wallis test followed by Dunn's multiple-comparison test (two-tailed) for data not following Gaussian distribution. A  $p$  value  $\leq 0.05$  was considered significant. Whole-cell current decays as depicted in Fig. 1a were fit to the built-in equation for a two-phase exponential decay provided by GraphPad Prism, using the constraints  $Y_0 (I_M/I_{M, \text{initial}} \text{ after } 0 \text{ min}) = 1$  and  $Y_{\text{plateau}} (I_M/I_{M, \text{initial}} \text{ after infinite minutes}) > 0$ .

Evaluation of synergy or antagonism between extracellular  $H^+$  and  $Na^+$  on ENaC sodium self-inhibition (SSI) was performed with the R-based synergyfinder package (<https://synergyfinder.fimm.fi>)<sup>3</sup> (50). Oocytes were exposed to six concentrations of  $Na^+$  (3, 10, 30, 60, 90, and 120 mM) at four different extracellular pH values (pH 8.0, 7.4, 7.0, and 6.0), and the degree of SSI was determined as relative fractions of ENaC inhibition. pH values were expressed as proton concentration in millimolar. To quantify the degree of  $H^+/Na^+$  interaction, SSI "inhibitory values" ranging from 0 (no inhibition) to 100 (full inhibition) were used as input for the synergy finder tool employing the Bliss synergy reference model (22). Interaction scores were visualized as three-dimensional interaction surfaces according to Ref. 50 with negative Bliss values indicating antagonism and positive values indicating

synergy. All figures were assembled and finalized using Inkscape (version 0.92.3; <https://inkscape.org>).<sup>3</sup>

**Author contributions**—L. W. and M. A. conceptualization; L. W. and S. M. data curation; L. W., J. M.-W., S. M., P. P. S., and M. A. formal analysis; L. W. and S. M. validation; L. W., J. S. D., J. M.-W., and S. M. investigation; L. W. and J. M.-W. visualization; L. W., P. P. S., and M. A. methodology; L. W. and M. A. writing-original draft; L. W., J. S. D., J. M.-W., S. M., P. P. S., I. M., and M. A. writing-review and editing; I. M. and M. A. resources; M. A. supervision; M. A. funding acquisition; M. A. project administration.

**Acknowledgments**—We thank Sean Gettings for generating ENaC cRNA and Dr. Tim Boswell as well as Dr. Peter Simmons for critical comments on the manuscript.

### References

1. Bayley, M., Damsgaard, C., Thomsen, M., Malte, H., and Wang, T. (2019) Learning to air-breathe: the first steps. *Physiology* **34**, 14–29 [CrossRef Medline](#)
2. Hanukoglu, I., and Hanukoglu, A. (2016) Epithelial sodium channel (ENaC) family: phylogeny, structure–function, tissue distribution, and associated inherited diseases. *Gene* **579**, 95–132 [CrossRef Medline](#)
3. Studer, R. A., Person, E., Robinson-Rechavi, M., and Rossier, B. C. (2011) Evolution of the epithelial sodium channel and the sodium pump as limiting factors of aldosterone action on sodium transport. *Physiol. Genomics* **43**, 844–854 [CrossRef Medline](#)
4. Kerem, E., Bistrizter, T., Hanukoglu, A., Hofmann, T., Zhou, Z., Bennett, W., MacLaughlin, E., Barker, P., Nash, M., Quittell, L., Boucher, R., and Knowles, M. R. (1999) Pulmonary epithelial sodium-channel dysfunction and excess airway liquid in pseudohypoaldosteronism. *N. Engl. J. Med.* **341**, 156–162 [CrossRef Medline](#)
5. Cogswell, M. E., Zhang, Z., Carriquiry, A. L., Gunn, J. P., Kuklina, E. V., Saydah, S. H., Yang, Q., and Moshfeh, A. J. (2012) Sodium and potassium intakes among US adults: NHANES 2003–2008. *Am. J. Clin. Nutr.* **96**, 647–657 [CrossRef Medline](#)
6. Giraldez, T., Rojas, P., Jou, J., Flores, C., and Alvarez de la Rosa, D. (2012) The epithelial sodium channel  $\delta$ -subunit: new notes for an old song. *Am. J. Physiol. Renal Physiol.* **303**, F328–F338 [CrossRef Medline](#)
7. Noreng, S., Bharadwaj, A., Posert, R., Yoshioka, C., and Bacongus, I. (2018) Structure of the human epithelial sodium channel by cryo-electron microscopy. *Elife* **7**, e39340 [CrossRef Medline](#)
8. Kellenberger, S., and Schild, L. (2002) Epithelial sodium channel/degenerin family of ion channels: a variety of functions for a shared structure. *Physiol. Rev.* **82**, 735–767 [CrossRef Medline](#)
9. Tavernarakis, N., and Driscoll, M. (1997) Molecular modeling of mechanotransduction in the nematode *Caenorhabditis elegans*. *Annu. Rev. Physiol.* **59**, 659–689 [CrossRef Medline](#)
10. Cottrell, G. (1997) The first peptide-gated ion channel. *J. Exp. Biol.* **200**, 2377–2386 [Medline](#)
11. Boscardin, E., Aljjevic, O., Hummler, E., Frateschi, S., and Kellenberger, S. (2016) The function and regulation of acid-sensing ion channels (ASICs) and the epithelial  $Na^+$  channel (ENaC): IUPHAR Review 19. *Br. J. Pharmacol.* **173**, 2671–2701 [CrossRef Medline](#)
12. Dymowska, A. K., Boyle, D., Schultz, A. G., and Goss, G. G. (2015) The role of acid-sensing ion channels in epithelial  $Na^+$  uptake in adult zebrafish (*Danio rerio*). *J. Exp. Biol.* **218**, 1244–1251 [CrossRef Medline](#)
13. Dymowska, A. K., Schultz, A. G., Blair, S. D., Chamot, D., and Goss, G. G. (2014) Acid-sensing ion channels are involved in epithelial  $Na^+$  uptake in the rainbow trout *Oncorhynchus mykiss*. *Am. J. Physiol. Cell Physiol.* **307**, C255–C265 [CrossRef Medline](#)
14. Collier, D. M., and Snyder, P. M. (2009) Extracellular protons regulate human ENaC by modulating  $Na^+$  self-inhibition. *J. Biol. Chem.* **284**, 792–798 [CrossRef Medline](#)

<sup>3</sup> Please note that the JBC is not responsible for the long-term archiving and maintenance of this site or any other third party hosted site.

## pH-sensitivity of *Xenopus* $\delta$ -ENaC

15. Coric, T., Zheng, D., Gerstein, M., and Canessa, C. M. (2005) Proton sensitivity of ASIC1 appeared with the rise of fishes by changes of residues in the region that follows TM1 in the ectodomain of the channel. *J. Physiol.* **568**, 725–735 [CrossRef Medline](#)
16. Lynagh, T., Mikhaleva, Y., Colding, J. M., Glover, J. C., and Pless, S. A. (2018) Acid-sensing ion channels emerged over 600 Mya and are conserved throughout the deuterostomes. *Proc. Natl. Acad. Sci. U.S.A.* **115**, 8430–8435 [CrossRef Medline](#)
17. Babini, E., Geisler, H. S., Siba, M., and Gründer, S. (2003) A new subunit of the epithelial Na<sup>+</sup> channel identifies regions involved in Na<sup>+</sup> self-inhibition. *J. Biol. Chem.* **278**, 28418–28426 [CrossRef Medline](#)
18. Wichmann, L., Vowinkel, K. S., Perniss, A., Manzini, I., and Althaus, M. (2018) Incorporation of the  $\delta$ -subunit into the epithelial sodium channel (ENaC) generates protease-resistant ENaCs in *Xenopus laevis*. *J. Biol. Chem.* **293**, 6647–6658 [CrossRef Medline](#)
19. Sheng, S., Carattino, M. D., Bruns, J. B., Hughey, R. P., and Kleyman, T. R. (2006) Furin cleavage activates the epithelial Na<sup>+</sup> channel by relieving Na<sup>+</sup> self-inhibition. *Am. J. Physiol. Physiol.* **290**, F1488–F1496 [CrossRef Medline](#)
20. Bize, V., and Horisberger, J. D. (2007) Sodium self-inhibition of human epithelial sodium channel: selectivity and affinity of the extracellular sodium sensing site. *Am. J. Physiol. Renal Physiol.* **293**, F1137–F1146 [CrossRef Medline](#)
21. Anantharam, A., Tian, Y., and Palmer, L. G. (2006) Open probability of the epithelial sodium channel is regulated by intracellular sodium. *J. Physiol.* **574**, 333–347 [CrossRef Medline](#)
22. Yadav, B., Wennerberg, K., Aittokallio, T., and Tang, J. (2015) Searching for drug synergy in complex dose-response landscapes using an interaction potency model. *Comput. Struct. Biotechnol. J.* **13**, 504–513 [CrossRef Medline](#)
23. Kashlan, O. B., Blobner, B. M., Zuzek, Z., Tolino, M., and Kleyman, T. R. (2015) Na<sup>+</sup> inhibits the epithelial Na<sup>+</sup> channel by binding to a site in an extracellular acidic cleft. *J. Biol. Chem.* **290**, 568–576 [CrossRef Medline](#)
24. Liu, W., Chun, E., Thompson, A. A., Chubukov, P., Xu, F., Katritch, V., Han, G. W., Roth, C. B., Heitman, L. H., IJzerman, A. P., Cherezov, V., and Stevens, R. C. (2012) Structural basis for allosteric regulation of GPCRs by sodium ions. *Science* **337**, 232–236 [CrossRef Medline](#)
25. Harding, M. M. (2002) Metal-ligand geometry relevant to proteins and in proteins: sodium and potassium. *Acta Crystallogr. D Biol. Crystallogr.* **58**, 872–874 [CrossRef Medline](#)
26. Li, T., Yang, Y., and Canessa, C. M. (2010) Two residues in the extracellular domain convert a nonfunctional ASIC1 into a proton-activated channel. *Am. J. Physiol. Cell Physiol.* **299**, C66–C73 [CrossRef Medline](#)
27. Li, T., Yang, Y., and Canessa, C. M. (2010) Leu85 in the  $\beta$ 1– $\beta$ 2 linker of ASIC1 slows activation and decreases the apparent proton affinity by stabilizing a closed conformation. *J. Biol. Chem.* **285**, 22706–22712 [CrossRef Medline](#)
28. Collier, D. M., Peterson, Z. J., Blokhin, I. O., Benson, C. J., and Snyder, P. M. (2012) Identification of extracellular domain residues required for epithelial Na<sup>+</sup> channel activation by acidic pH. *J. Biol. Chem.* **287**, 40907–40914 [CrossRef Medline](#)
29. Ji, H.-L., and Benos, D. J. (2004) Degenerin sites mediate proton activation of  $\delta\beta\gamma$ -epithelial sodium channel. *J. Biol. Chem.* **279**, 26939–26947 [CrossRef Medline](#)
30. Zhang, P., Fyfe, G. K., Grichtchenko, I. I., and Canessa, C. M. (1999) Inhibition of  $\alpha\beta$  epithelial sodium channels by external protons indicates that the second hydrophobic domain contains structural elements for closing the pore. *Biophys. J.* **77**, 3043–3051 [CrossRef Medline](#)
31. Palmer, L. G., and Frindt, G. (1987) Effects of cell Ca<sup>2+</sup> and pH on Na<sup>+</sup> channels from rat cortical collecting tubule. *Am. J. Physiol.* **253**, F333–F339 [CrossRef Medline](#)
32. Chalfant, M. L., Denton, J. S., Berdiev, B. K., Ismailov, I. I., Benos, D. J., and Stanton, B. A. (1999) Intracellular H<sup>+</sup> regulates the  $\alpha$ -subunit of ENaC, the epithelial Na<sup>+</sup> channel. *Am. J. Physiol.* **276**, C477–C486 [CrossRef Medline](#)
33. Awayda, M. S., Boudreaux, M. J., Reger, R. L., and Hamm, L. L. (2000) Regulation of the epithelial Na<sup>+</sup> channel by extracellular acidification. *Am. J. Physiol. Cell Physiol.* **279**, C1896–C1905 [CrossRef Medline](#)
34. Humphreys, B. D., Jiang, L., Chernova, M. N., and Alper, S. L. (1994) Functional characterization and regulation by pH of murine AE2 anion exchanger expressed in *Xenopus* oocytes. *Am. J. Physiol.* **267**, C1295–C1307 [CrossRef Medline](#)
35. Assmann, M., Kuhn, A., Dürrnagel, S., Holstein, T. W., and Gründer, S. (2014) The comprehensive analysis of DEG/ENaC subunits in *Hydra* reveals a large variety of peptide-gated channels, potentially involved in neuromuscular transmission. *BMC Med.* **12**, 84 [CrossRef Medline](#)
36. Ji, H. L., Su, X. F., Kedar, S., Li, J., Barbry, P., Smith, P. R., Matalon, S., and Benos, D. J. (2006)  $\delta$ -Subunit confers novel biophysical features to  $\alpha\beta\gamma$ -human epithelial sodium channel (ENaC) via a physical interaction. *J. Biol. Chem.* **281**, 8233–8241 [CrossRef Medline](#)
37. Evans, B. J., Carter, T. F., Greenbaum, E., Gvoždík, V., Kelley, D. B., McLaughlin, P. J., Pauwels, O. S., Portik, D. M., Stanley, E. L., Tinsley, R. C., Tobias, M. L., and Blackburn, D. C. (2015) Genetics, morphology, advertisement calls, and historical records distinguish six new polyploid species of African clawed frog (*Xenopus*, Pipidae) from West and Central Africa. *PLoS ONE* **10**, e0142823 [CrossRef Medline](#)
38. Kashlan, O. B., Balchak, D. M., Gentilcore, C., and Clark, N. L. (2018) Cleavage of ENaC  $\alpha$  and  $\gamma$  subunits evolved with the terrestrial migration. *FASEB J.* **32** (Abstr 624.16)
39. Collier, D. M., Tomkovicz, V. R., Peterson, Z. J., Benson, C. J., and Snyder, P. M. (2014) Intersubunit conformational changes mediate epithelial sodium channel gating. *J. Gen. Physiol.* **144**, 337–348 [CrossRef Medline](#)
40. Leaf, A., Keller, A., and Dempsey, E. F. (1964) Stimulation of sodium transport in toad bladder by acidification of mucosal medium. *Am. J. Physiol.* **207**, 547–552 [CrossRef Medline](#)
41. Ussing, H. H. (1949) The active ion transport through the isolated frog skin in the light of tracer studies. *Acta Physiol. Scand.* **17**, 1–37 [CrossRef Medline](#)
42. Steinmetz, P. R. (1974) Cellular mechanisms of urinary acidification. *Physiol. Rev.* **54**, 890–956 [CrossRef Medline](#)
43. Frazier, L. W., and Vanatta, J. C. (1971) Excretion of H<sup>+</sup> and NH<sub>4</sub><sup>+</sup> by the urinary bladder of the acidotic toad and the effect of short-circuit current on the excretion. *Biochim. Biophys. Acta* **241**, 20–29 [CrossRef Medline](#)
44. Balinsky, J. B., and Baldwin, E. (1961) The mode of excretion of ammonia and urea in *Xenopus laevis*. *J. Exp. Biol.* **38**, 695–705
45. McBean, R. L., and Goldstein, L. (1970) Renal function during osmotic stress in the aquatic toad *Xenopus laevis*. *Am. J. Physiol.* **219**, 1115–1123 [CrossRef Medline](#)
46. McClanahan, L., Jr. (1967) Adaptations of the spadefoot toad *Scaphiopus couchi*, to desert environments. *Comp. Biochem. Physiol.* **20**, 73–99 [CrossRef](#)
47. Shoemaker, V. H. (1964) The effects of dehydration on electrolyte concentrations in a toad, *Bufo marinus*. *Comp. Biochem. Physiol.* **13**, 261–271 [CrossRef Medline](#)
48. Yang, J., Yan, R., Roy, A., Xu, D., Poisson, J., and Zhang, Y. (2015) The I-TASSER Suite: protein structure and function prediction. *Nat. Methods* **12**, 7–8 [CrossRef Medline](#)
49. Sievers, F., Wilm, A., Dineen, D., Gibson, T. J., Karplus, K., Li, W., Lopez, R., McWilliam, H., Remmert, M., Söding, J., Thompson, J. D., and Higgins, D. G. (2011) Fast, scalable generation of high-quality protein multiple sequence alignments using Clustal Omega. *Mol. Syst. Biol.* **7**, 539 [CrossRef Medline](#)
50. Ianevski, A., He, L., Aittokallio, T., and Tang, J. (2017) SynergyFinder: a web application for analyzing drug combination dose-response matrix data. *Bioinformatics* **33**, 2413–2415 [CrossRef Medline](#)
51. Corpet, F. (1988) Multiple sequence alignment with hierarchical clustering. *Nucleic Acids Res.* **16**, 10881–10890 [CrossRef Medline](#)